Journal of Materials Chemistry A

Rethinking Sodium-Ion Anodes as Nucleation Layers for Anode-Free Batteries

Journal:	*Journal of Materials Chemistry A*
Manuscript ID	TA-ART-06-2018-005911.R1
Article Type:	Paper
Date Submitted by the Author:	03-Nov-2018
Complete List of Authors:	Cohn, Adam; Vanderbilt University, Mechanical Engineering Metke, Thomas; Vanderbilt University, Mechanical Engineering Donohue, Jennifer; Vanderbilt University, Mechanical Engineering Muralidharan, Nitin; Vanderbilt University, Materials Science Share, Keith; Vanderbilt University, Materials Science Pint, Cary; Vanderbilt University, Mechanical Engineering

Rethinking Sodium-Ion Anodes as Nucleation Layers for Anode-Free Batteries

Adam P. Cohn[1], Thomas Metke[1], Jennifer Donohue[1], Nitin Muralidharan[2], Keith Share[2], and Cary L. Pint[1,2,]*

[1]Department of Mechanical Engineering, Vanderbilt University, Nashville, TN 37235

[2]Interdisciplinary Materials Science Program, Vanderbilt University, Nashville, TN 37235

*Electronic mail: cary.l.pint@vanderbilt.edu

Keywords

anode-free, sodium metal battery, sodium anode, sodium nucleation, sodium-free, anode-less, diglyme, energy efficiency

Abstract

Here we report a room-temperature sodium metal battery, where the sodium initially stored in a $Na_3V_2(PO_4)_3$ cathode is plated, upon charging, onto an aluminum current collector coated with a thin nucleation layer. To maximize the battery performance, conventional sodium-ion anode materials, including non-graphitized carbons and sodium-alloying metals, were evaluated as nucleation layers to facilitate stable electroplating of sodium metal. Among several materials studied, carbon black and bismuth showed the highest sodium plating-stripping Coulombic efficiencies in half-cell testing, averaging 99.9% and 99.85%, respectively, over 50 cycles at 0.5 mA/cm^2. Building on these findings, anode-free cells with $Na_3V_2(PO_4)_3$ cathodes were assembled in a discharged state, demonstrating energy densities up to 318 Wh/kg at 0.25 mA/cm^2 (~C/6), a first-cycle Coulombic efficiency up to 92%, a stable discharge voltage at 3.35 V, an average round-trip energy efficiency of 98%, and a capacity retention of 82.5% after 100 cycles at 0.5 mA/cm^2 (~C/3). With its unique performance highlighted in this work, the anode-free sodium battery emerges as a low-cost, high-performance option for stationary electric storage.

1. Introduction

Lithium-ion batteries (LIBs) are being increasingly deployed for stationary electric storage due to a rapid decline in cell costs and rise of intermittent renewable generation. Sodium-ion batteries (SIBs), in a form analogous to LIBs, have attracted a resurgence of academic research over the last decade, with the goal of achieving a battery that is more cost-effective than LIBs, and accordingly even better suited for stationary electric storage. SIB research has been in part motivated by the great natural abundance of sodium, in contrast to the more limited global supply of cobalt and lithium used in LIBs,[1] and the stability of sodium with lower-cost aluminum negative current collectors. However, to reduce cell costs per kilowatt-hour (kWh), both raw material costs and energy density must be considered.[2] In this respect, it remains unclear if SIBs can provide a sufficient material cost savings to compensate for their lower energy density, and reach cell costs per kWh below state-of-the-art LIBs, jeopardizing prospects for commercialization.[3, 4]

While SIB energy density has progressed with the discovery of new electrode materials, mainly with reports on new oxide compounds[5, 6] and polyanion compounds[7-11] for the cathode material, advancements on the anode material have been limited until recently. Since sodium differs from lithium and potassium and does not form a binary graphite intercalation compound, such as LiC_6 or KC_8, with significant ion-storage capacity,[12] SIB development has required the use of alternative anodes.[13] Hard carbon is considered to be one of the best-suited materials to fill this role, offering a capacity up to 300 mAh/g, although its high first-cycle sodium loss is problematic for SIB development.[14, 15] In the effort to mitigate this issue, researchers have replaced carbonate-based electrolytes with ether-based electrolytes and demonstrated improved first-cycle performance for non-graphitized carbons.[16, 17] The increased stability offered by such electrolytes has also enabled the cointercalation of sodium ions and solvent into graphitized carbons, with remarkably fast kinetics and stable cycling, but a limited capacity (<150 mAh/g).[18, 19] In addition, ether-based electrolytes are also reported to improve the cycling performance of alloying anodes, such as tin (forming $Na_{15}Sn_4$, 847 mAh/g_{Sn}) and bismuth (forming Na_3Bi, 385 mAh/g_{Bi}),[20, 21] and even to facilitate the stable plating and stripping of sodium metal.[22] Underlying these findings is the higher LUMO (Lowest Unoccupied Molecular Orbital) level of ether-based electrolytes (in comparison to carbonates),[23] and the lower electrochemical potential of sodium (in comparison to lithium). Among this range of anodes which show enhanced performance in ether-based electrolytes, sodium metal stands out with respect to energy density, as it offers the greatest capacity and voltage. However, the difficulty in processing sodium films[24] and their reactivity in air would make the manufacturing of such sodium metal batteries challenging.

To maximize energy density without sacrificing manufacturability, we have proposed the use of an anode-free design, where the cell is assembled in a discharged state with all the sodium contained in the cathode. While a similar approach was originally demonstrated for thin-film lithium batteries using a LiPON electrolyte,[25] efforts to adapt this concept for high energy density lithium cells have proved difficult due to the limited Coulombic efficiency of lithium plating and stripping, and the resulting rapid loss of capacity.[26] In contrast, the high Coulombic efficiency of sodium plating and stripping in ether-based electrolytes makes this a promising approach for developing a sodium metal battery. Toward this goal, our group recently showed that a thin layer of carbon (the nucleation layer) allowed us to use an aluminum negative current collector, rather than the denser and more costly copper current collector used in Ref. 22, and achieve highly stable sodium plating and stripping.[27] However, many important factors of a practical anode-free cell architecture remain unexplored including the role of the nucleation layer in controlling Coulombic efficiency and first cycle loss as well as practical methods to achieve air-stable cell architectures compatible with conventional battery manufacturing routes that maintain high energy density.

Here, we present a study that explores (1) how the nucleation layer composition impacts sodium plating-stripping performance, and (2) how this can be utilized in an anode-free configuration with an air-stable cathode. In the first case, we reevaluate materials known to be stable SIB anodes in ether-based electrolytes as nucleation layers for sodium plating. Our electrochemical testing reveals that the energetics of sodium nucleation and the resulting Coulombic efficiency are dependent on the nucleation layer composition, opening pathways to engineer this layer to minimize sodium loss and maximize cycle life. In addition, we show that the use of a nucleation layer, in contrast to an insertion anode, can significantly reduce the first-cycle loss, allowing the anode-free design to overcome a key challenge facing SIB development. Finally, anode-free cells are assembled using the polyanionic cathode $Na_3V_2(PO_4)_3$, demonstrating energy densities 40% greater than previously reported SIBs with this cathode material[20] and unprecedented round-trip energy efficiencies, averaging 98% over 100 cycles. Our work highlights new design strategies for developing an anode-free sodium battery—a device architecture that may prove to be the most practical approach to reaching the energy densities required for a sodium-based battery to become commercially viable.

2. Results and Discussion

2.1 Evaluating Anode Materials as Nucleation Layers

A SIB and an anode-free sodium battery using a nucleation layer are both illustrated in Figure 1a. In contrast to a SIB, the anode-free battery is intentionally unbalanced, and operates through the plating and stripping of sodium metal on the nucleation layer at the negative electrode.

The use of a nucleation layer, as opposed to plating directly on the Al current collector, stabilizes the plating and stripping of sodium (alleviating problems of sodium delamination and dendritic growth) and increases the Coulombic efficiency.[27] The designation of anode-free is derived from the lack of a host anode material on the negative electrode that is common in conventional battery systems. In this study, we focus on a series of materials that exhibit stable performance in ether-based electrolytes as insertion anodes, and reconsider their utility as nucleation layers. It is, however, important to make the distinction that, unlike in the case of SIB design, the mass loading of the nucleation layer (mg/cm^2) does not limit the capacity (mAh/cm^2) of the cell, and the composition of the nucleation layer does not significantly alter the operating voltage or energy density of the cell. Accordingly, the ideal nucleation layer will consist of a thin coating composed of a material that maximizes the stability and lifetime of the cell.

Figure 1b shows the energy density of different negative electrodes paired with a $Na_3V_2(PO_4)_3$ cathode, including the anode-free configuration. The calculated gravimetric energy densities, E, presented in Figure 1b (patterned gray bars in the plot) were determined using the following relationship:

$$E = \frac{Q_{Cathode} \times Q_{Anode}}{Q_{Cathode} + Q_{Anode}} \times (V_{Cathode} - V_{Anode}) \qquad (1)$$

where Q is the electrode capacity and V is the average operating voltage with respect to sodium metal. The specific Q and V values used in these calculations are presented in Table S1. The reported energy densities (solid gray bars in the plot) are from recent work conducted by Tarascon and coworkers.[20] The maximum gravimetric energy density of 388 Wh/kg for the anode-free cell is calculated assuming the mass of the nucleation layer is 1% of the mass of the cathode. The 318 Wh/kg demonstrated in this work is notably 40% higher than the recently reported value for the tin//$Na_3V_2(PO_4)_3$ cell.[20] In addition, considering the density of the active materials, we calculate that the anode-free approach can provide a >100% increase in volumetric energy density compared to a sodium-ion cell (Table S2). In this respect, it is important to highlight that recent reports have pointed out that the low density of sodium-ion anodes poses a key challenge to SIB feasibility.[4, 28] Accordingly, despite the inherent challenges that come with developing a new battery system, the potential of the anode-free approach to provide significant gains in gravimetric and volumetric energy densities serves as strong motivation to research this system.

To evaluate the performance and nucleation energetics of the different nucleation layer compositions, electrochemical testing was conducted in half cells using sodium metal as the counter and reference electrode and an electrolyte of 1M $NaPF_6$ in diethylene glycol dimethyl ether (diglyme). Carbon black and hard carbon were first selected for comparison because they exhibit different sodium-ion storage properties despite their similar defective nature. X-ray diffraction patterns for the synthesized hard carbon and the purchased carbon black are presented in Figure S1. As shown in the insertion-extraction profiles in Figures 2a and b, hard carbon exhibited approximately three times the sodium-ion storage capacity of carbon black. The hard carbon plateau at 0.1 V, which accounts for the increased capacity, has controversially been attributed to either the adsorption of sodium ions in carbon micropores or the intercalation of sodium ions between graphene sheets.[14, 29]

The energy barrier to sodium nucleation was measured by plating (allowing the voltage to drop below 0 V vs. Na/Na^+) on fully sodiated electrodes at a low current density of 40 $\mu A/cm^2$ to minimize the effect of mass transfer.[30] We found that the nucleation overpotential (Figures 2c and d) was significantly lower for the hard carbon (6 mV) than the carbon black electrode (13 mV). This difference may be explained in part by the different operating voltages of the sodium ion storage in the different carbon materials. The lower operating voltage of the sodium ion storage in hard carbon indicates a lower degree of ionicity of the stored sodium,[31] resulting in an electrode that is more similar to sodium metal. Accordingly, the nucleation overpotential is lower on such an electrode, which is expected to result in smaller and more numerous sodium nuclei, as the nuclei critical radius is dependent on the energy barrier as described in classical nucleation theory.[32]

To assess the sodium plating-stripping performance, testing was conducted at an increased current density of 0.5 mA/cm^2, a plating capacity of 0.5 mAh/cm^2, and a stripping cutoff of 50 mV. Figures 2e and f show 50 plating-stripping cycles performed on the carbon black and hard carbon electrodes with the start of each cycle plotted from the capacity endpoint of the previous cycle in order to capture the slippage due to the loss of charge. This form of plot, which has been utilized by Dahn's group to analyze full cells,[33] highlights the total conservation of charge while also showing all the cycle profiles in entirety. Loss of charge, with Coulombic efficiencies deviating from unity, results in a cycle-to-cycle shift to the right. In this manner, the difference in the starting and ending point after 50 cycles corresponds to the cumulative loss of charge. While both electrodes exhibited stable performance, the carbon black electrode exhibited approximately half the charge loss over the 50 cycles than the hard carbon electrode, with respective charge losses of 0.026 mAh/cm^2 and 0.054 mAh/cm^2. The corresponding average Coulombic efficiencies were calculated to be 99.90% for the carbon black electrode and 99.78% for the hard carbon electrode. It is important to point out that although this difference may appear insignificant, it was observed to be relatively consistent across multiple devices tested (Figure S2), and is very meaningful for developing anode-free cells, where the loss of sodium is expected to be the limiting factor for cycle life.

Next, tin and bismuth were selected for comparison as alloying electrodes because they show different sodium alloying behavior and they have both been recently reported to exhibit stable performance as alloying anodes in diglyme-based electrolytes.[20, 21] Electrodes were prepared with microsized particles (325 mesh) in accordance with these previous reports. Figures 3a and b show the voltage profiles performed at 0.1 A/g between 0 and 2 V vs. Na/Na^+. The bismuth alloying curve displays flat plateaus at 0.7 and 0.5 V, with the lower voltage plateau reaching twice the capacity of the higher voltage plateau. These two distinct plateaus have been identified as the formation of NaBi and Na_3Bi alloys, which is in agreement with the capacity of ~380 mAh/g. In contrast, the tin alloying curve shows more than twice the capacity, approximately forming $Na_{15}Sn_4$, and less distinct plateaus that are closer to the Na/Na^+ potential.

Figures 3c and d show the voltage profiles for the nucleation of sodium metal on these alloys. The nucleation overpotentials for the sodium-bismuth alloy and the sodium-tin alloy are 3 mV and less than 1 mV, respectively. The difference between the two nucleation overpotentials can again be explained in part by the difference in operating voltage of the initial alloying process, with the formation of the sodium-tin alloy taking place closer to the potential of Na/Na^+. In addition, the higher sodium content of the sodium-tin alloy can be interpreted as making the alloy more sodium-like.

Where the small barrier to nucleation measured for the sodium-bismuth alloy suggests the initial formation of small sodium nuclei, the absence of a barrier to nucleation on the sodium-tin alloy may indicate layered growth. From the corresponding 50 cycles of plating-stripping shown in Figures 3e and f, it is clear that the sodium-bismuth electrode demonstrated less charge loss than the sodium-tin electrode. Average Coulombic efficiencies were calculated to be 99.85% and 99.63% for the bismuth and tin alloying electrodes, respectively. Interestingly, the carbon black and the bismuth electrodes, which showed the comparatively lower capacities and higher operating voltages for sodium-ion storage, facilitated improved Coulombic efficiencies for the plating and stripping of sodium metal. These findings provide evidence of a correlation between higher energy barriers to nucleation and higher sodium metal plating-striping Coulombic efficiencies. We attribute this correlation to the differing nuclei size, and resulting plating morphology, as this is dependent on the energy barrier to form critical nuclei.[32] Specifically, we propose that sodium metal depositions with higher surface-area-to-volume ratios, corresponding to lower measured nucleation overpotentials and smaller nuclei sizes, are likely to result in more parasitic reactions with the electrolyte than depositions with lower surface-area-to-volume ratios, corresponding to higher measured nucleation overpotentials and larger nuclei sizes. However, it is important to point out that we previously showed that plating on materials exhibiting very high nucleation overpotentials, such as bare aluminum, can result in more severe concerns, including: (1) delamination due to poor mechanical connectivity between the sodium and the electrode; and (2) problematic dendritic growth due to the high effective current densities produced by non-uniform and poorly-spread sodium depositions.[27] In this respect, our use of nucleation layers allows us to overcome these highly problematic events and probe the more subtle differences in Coulombic efficiency that appear to be due to differing nucleation energetics and resulting morphologies. In contrast, recent work examining nitrogen-doped graphene[34] and carbon nanofibers with silver nanoparticles[35] as nucleation layers for lithium plating, have been mainly limited to alleviating dendritic growth. By assessing the sodium-ion storage properties, the sodium metal nucleation energetics, and the Coulombic efficiency of sodium metal plating and stripping for these different materials, we were able to develop a more comprehensive understanding of the preferred properties of a sodium nucleation layer that is critical to the development of anode-free cells.

While all of the tested electrodes exhibited high Coulombic efficiencies and stable performance, carbon black was selected as the nucleation layer for anode-free cells because it demonstrated the highest Coulombic efficiency. Testing to evaluate carbon materials with significantly higher and significantly lower surface areas than carbon black was also conducted using natural graphite and activated carbon, respectively, but neither offered improved performance in comparison to the carbon black (Figure S3). Additional testing using carbon black nucleation layers was performed to evaluate the potential for dendritic growth[36] and the resting stability of the plated sodium metal. While the cycling profiles in Figures 2 and 3 show no electrochemical evidence of problematic dendritic growth, we conducted an additional plating test to determine if evidence of dendrites can be observed with higher plating capacities. We found that over 30 mAh/cm^2 of sodium metal could be deposited at a current of 1 mA/cm^2 while maintaining a stable voltage profile (Figure S4). Opening the cell afterwards, a smooth, shiny film of sodium metal was observed on the working electrode, with all of the sodium metal removed from the counter electrode (Figure S4). Such sodium metal films form after individual flat islands of sodium metal (shown in Figure S5) grow and coalesce together. Testing was also conducted to probe the resting stability of the plated sodium metal to assess the potential for cell discharge. After introducing a 10-hour rest period between plating and stripping steps, an average Coulombic efficiency of 99.73% was maintained (Figure S6), indicating good resting stability.

2.2 Mitigating First-Cycle Loss

The first-cycle loss of capacity at the negative electrode presents a significant challenge to many new battery chemistries. This is particularly problematic in the case of SIB development, where hard carbon anodes consume at least 15% of the sodium content during the first cycle. While numerous techniques have been proposed to help alleviate this issue, such as pre-charging the anode, adding excess sodium/lithium to the cathode, and using sacrificial salts, it remains unclear if these techniques can be practically applied for scaled-up manufacturing.[37, 38] Moreover, increasing the mass loading of the cathode is not considered a practical approach to compensate for the loss of sodium because this may result in the unintended plating of sodium metal.[15] However, the unbalanced design of the anode-free cell allows us to overcome this key challenge. Although there is first-cycle loss in the anode-free cell that results from the initial sodiation of the nucleation layer and the formation of a solid electrolyte interphase (SEI) layer, the percent loss can be simply reduced by increasing the areal loading of the cathode. In figure 4, we illustrate this distinction between an insertion anode and a nucleation layer using half-cell testing. Figure 4a shows the first-cycle profile for hard carbon, exhibiting a 16% first-cycle loss. Importantly, this percent will not significantly change with areal loading. In contrast, Figure 4b shows the first-cycle profile for a carbon black nucleation layer (0.25 mg/cm^2), exhibiting only 3.5% first-cycle loss after plating 2 mAh/cm^2. As expected, we observed that this percent loss is dependent on the plating capacity, with lower capacities showing a greater percent loss (Figure S7). In the context of commercial cells, with cathode areal loadings greater than 2 mAh/cm^2, this unique feature of the anode-free approach will be highly advantageous and allow for higher achievable energy densities.

2.3 Anode-Free Battery with $Na_3V_2(PO_4)_3$ Cathodes

In choosing a cathode to demonstrate the anode-free approach, it was important to select an air-stable material that is not sodium deficient to allow for facile processing. With the target of reaching LIB performance, we also sought a cathode to allow for extended cycling, a high energy density, a stable discharge voltage, and stability in the electrochemical window of the 1M $NaPF_6$ in diglyme electrolyte (Figure S8). After careful consideration, we selected $Na_3V_2(PO_4)_3$: a

NASICON compound with an open 3D structure that allows for rapid sodium-ion conduction. Specifically, carbon-coated $Na_3V_2(PO_4)_3$ nanoparticles were prepared using a solid-state synthesis after wet ball-milling of the precursors.[39] Figures 5a and 5b show the synthesized particles and the corresponding x-ray diffraction pattern which can be indexed to the R3-C space group with a NASICON structure. To evaluate the cathode properties, half-cell testing was conducted using 1M $NaPF_6$ in diglyme. Figure 5c shows one full cycle between the range of 3.0 and 3.7 V vs. Na/Na^+. The measured capacity of 105 mAh/g is about 90% of the theoretical capacity of 117 mAh/g. The stable discharge voltage at ~3.35 V provides a cathode-specific energy density of ~350 Wh/kg. The low voltage hysteresis of 30 mV at a rate of C/6 is less than one hundredth of the operating voltage, allowing for round-trip energy efficiencies approaching 99%. In addition, half-cell cycling without significant capacity decay over 100 cycles is shown in Figure S9.

Anode-free cells were assembled and tested (Figure 6) using carbon black (~0.2 mg/cm^2) on Al foil as the negative electrode and $Na_3V_2(PO_4)_3$ (~12 mg/cm^2) on Al foil as the positive electrode. To achieve mass loadings of >10 mg/cm^2 without electrode cracking, isopropyl alcohol was added to the aqueous solution to reduce surface tension.[40] Importantly, no sodium metal was used in making these cells, and no modification to the electrodes were made such as pre-sodiation or pre-cycling. Accordingly, this design should allow for manufacturing in line with current methods employed for LIBs.

Figure 6b shows the first 20 cycles of an anode-free cell cycled galvanostatically at 0.25 mA/cm^2 (~C/6 with respect to the cathode) between 3.0 and 3.7 V. In the first cycle, starting at ~0.8 V, the carbon black nucleation layer is sodiated (taking place prior to the flat charging plateau). The transition from sodium-ion storage in the carbon black (SIB-like operation) to sodium plating is marked by a nucleation spike. In this first cycle, the nucleation spike appears small on the left shoulder of the charging curve (as shown in inset in Figure 6b), but then becomes more pronounced in the subsequent cycles. We attribute this to nucleation initially occurring prior to the cathode reaching its plateau. After sodium is lost in the first few cycles, the cathode is never fully sodiated, so the nucleation event aligns with the plateau, and as a result, it is more evident in the voltage profiles. It is also worth noting here that the presence of the nucleation spike observed at the start of each charging step indicates that sodium metal is freshly plated on the nucleation layer during each cycle (Figure S10 shows how the magnitude of the nucleation spike evolves with cycling).

In the first cycle, the discharge capacity was 96 mAh/g with respect to the mass of the cathode, or 1.26 mAh/cm^2. The maximum energy density discharged was 318 Wh/kg with respect to the mass of the cathode and the nucleation layer. The first-cycle loss of 8% includes oxidation of the electrolyte at the cathode in addition to carbon sodiation and SEI formation at the nucleation layer. Stable performance is observed over the first 20 cycles with some evidence of electrolyte oxidation (slippage in the upper right corner of the plot), and additional loss of charge at the negative electrode (further slippage on the left side of the plot). Accordingly, the Coulombic efficiency that levels out around 99.4% after the first five cycles indicates minor parasitic reactions at both electrodes, rather than a direct loss of 0.6% sodium per cycle.

Figures 7a and b show the voltage profiles for cells cycled at 0.25 mA/cm^2 (~C/6) and 0.5 mA/cm^2 (~C/3) over 100 cycles, and the corresponding capacity retention with respect to cycle number. As in the half cell testing, it is important to point out that no electrochemical evidence of problematic dendritic growth is observed in these cycling voltage profiles. Over the first 100 cycles, the capacity retention was 70.4% and 82.5% for the devices cycled at 0.25 mA/cm^2 and 0.5 mA/cm^2, respectively. Additional plots of energy efficiency, Coulombic efficiency, and average charging/discharging voltages over the first 100 cycles are presented in Figures S11and S12. Since the cathode material exhibited stable performance in half-cell testing, we assume the capacity fade is primarily due to sodium loss. This assumption was later confirmed by removing the cathode from an anode-free cell and testing it in a half cell, with the cathode reverting back to full capacity (Figure S13). Accordingly, the capacity retention with respect to cycle number can be described as follows:

$$Q(n) = Q_0 \eta^n \quad (2)$$

where Q is the cell capacity as a function of cycle number, n, and Q_0 is the initial cell capacity, and η is the plating-stripping Coulombic efficiency. Decay curves for η = 99.9%, 99.8%, 99.7%, 99.6% and 99.5% are plotted for comparison. The η = 99.9% line corresponds to the Coulombic efficiency of the plating and stripping on carbon black nucleation layer measured in half cell testing. Our results approximately follow η =99.8% for the device cycled at 0.5 mA/cm^2 and η =99.65% for the device cycled at 0.25 mA/cm^2. The deviation from the half-cell testing may be due to changes in the electrolyte caused by the cathode and/or the deactivation of some sodium metal during cycling. The difference in cycling between the two rates can be attributed in part to cycling time,[41] as the device cycled at the slower rate cycled for approximately twice the duration, providing more time for parasitic reactions. In comparison, recent work testing anode-free lithium batteries with a $LiFePO_4$ cathode supplied by A123 and a highly concentrated electrolyte showed a capacity retention of ~35% after 100 cycles at 0.2 mA/cm^2,[26] corresponding to η < 99.0%, with cycling at 0.5 mA/cm^2 showing similar performance. The significantly improved capacity retention demonstrated in our work underscores the advantage of using a nucleation layer and the pairing of sodium with the 1M $NaPF_6$ in diglyme electrolyte. Further, improved performance in cycling these devices will occur synchronously with improvements in Coulombic efficiency, where our results demonstrate a clear correlation to the choice of a nucleation layer. It is also important to point out here that unlike cycling performed with an excess of cathode material or an excess of sodium metal, our cycling corresponds to 100% depth of discharge and reflects the underlying plating-stripping Coulombic efficiency as these cells are sodium limited.

Next, to better understand the observed capacity fade with cycling, the anode-free cells characterized in Figure 7 were disassembled in a fully charged state (3.7 V) after 100+ cycles and photographed (Figure 8). Here, we note a relatively uniform covering of the 1 cm diameter nucleation layers (black) with shiny sodium metal. As expected,[32] the islands of sodium appear smaller in the cell operated at higher current. Interestingly, sodium metal is also found adhered to the edges of the nucleation layer discs with patches of duller-gray sodium spread onto the larger stainless steel discs. Opening similar cells in a discharged state after extended cycling showed exterior sodium that was left behind. This presence of inactive sodium on the stainless steel discs may be due to the geometry of the assembled cells, which produces non-uniform current distributions at the edges of the electrodes. In addition, variations in pressure due to the stack arrangement and the crimping process can deform separators, and have been reported to result in spatial variations in deposition near the edges.[42] With some of the measured cell capacity loss explained by the spreading and deactivation of sodium, we expect that scaled-up devices will show improved cycling through the reduction of these edge effects and the use of higher aerial loading cathodes. In addition, the increased flexibility of a pouch cell format may also help alleviate this issue as it may better accommodate the volume change, which is ~20% with respect to the active materials (Table S2). Going forward, there are a range of promising routes to build on this work to further extend the cycle lives of these cells, including: increasing the Coulombic efficiency through the further optimization of the nucleation layer, developing an optimized charging protocol,[26] using high aerial loading cathodes,[43] and utilizing methods to incorporate excess sodium into the cells.[38] In turn, whereas we demonstrate 99.9% Coulombic efficiency, further improvement of nucleation layer properties, high areal loading of the cathode material, and other cell-level factors could lead to competitive stability of Na metal anodes relative to commercial Li-ion anode materials. This would facilitate cycling performance relevant to many emerging market opportunities where the synergy between low material and manufacturing cost, high energy density, and high durability is an ideal combination.

Finally, it is worthwhile to note additional unique battery attributes that are enabled by our anode-free approach that are particularly important for system-level integration. First, the voltage during discharge is remarkably stable, with 98% percent of the discharge occurring between 3.4 and 3.3 V when operated at 0.25 mA/cm^2 from 3.7 to 3.0 V. This capability to maintain a constant voltage during discharge may eliminate the need for power electronics (such as boost converters) at the system level that are costly and consume energy. Second, the round-trip energy efficiencies of the anode-free cells were found to be exceptionally high, with averages of 98.1% (0.5 mA/cm^2) and 98.0% (0.25 mA/cm^2) over 100 cycles. This feature is especially attractive in the context of stationary electric storage, where energy losses reduce the value of batteries as resources to the grid and accumulate to be significant over long operational lifetimes.[44] We also expect that such high energy efficiencies will allow for simpler and potentially less costly thermal management.

3. Conclusions and Future Directions

In this work, we demonstrate how rethinking the role of the negative electrode to function as a nucleation layer to initiate and direct sodium plating rather than acting an insertion anode can enable the development of a high-performance sodium metal battery assembled in an anode-free manner. This design leverages the inherent electrochemical stability of anode materials, the known electrochemical stability of sodium metal in ethers, and relies upon air-stable cathodes that can be processed into high energy density sodium batteries utilizing existing methods used in battery manufacturing. Specifically, our work demonstrates up to 99.9% Coulombic efficiency for sodium metal plating onto nucleation layers, where the properties of nuclei formation at the electrode-electrolyte interface controls the Coulombic efficiency. This presents a new mechanistic framework where classical nucleation theory combined with interfacial chemistry can be used to engineer improved Coulombic efficiency and cell level performance. Additionally, whereas the high first cycle capacity loss remains a key challenge to SIB development, we demonstrate here that the anode-free approach leads to over 4X lower first cycle loss compared to conventional hard carbons, with a total full cell first cycle loss of < 8% that can be decreased by thicker areal cathode loadings. For our full cell studies, we synthesize and demonstrate the use of $Na_3V_2(PO_4)_3$ in an anode-free cell with an energy density of 318 Wh/kg and flat operating voltage at 3.35 V. Moreover, this battery architecture boasts an average roundtrip energy efficiency at or above 98%, which can lead to significant cost savings for large-footprint energy storage systems relevant for grid storage or electric vehicles. Finally, anode-free cells cycled 100 times at 0.25 mA/cm^2 (~C/6) and 0.5 mA/cm^2 (~C/3), retained 70.4% and 82.5% of their initial capacity, respectively, with evidence that scaled-up cells are likely to exhibit improved cycling through the alleviation of edge effects. These results are of significant practical utility since all fabrication processes for these materials rely on techniques currently utilized in conventional battery manufacturing processes.

Moving forward, we envision that the anode-free approach can be tailored to achieve a range of performance goals and satisfy different design constraints. With respect to energy density, cathodes can be selected to provide up to 500 Wh/kg with options such as fluorophosphates with elevated operating voltages,[7] or nickel-containing O3-type layered oxides with higher capacities.[6,

[45] Our tests demonstrate 1 M $NaPF_6$ in diglyme to be stable until ~ 4.2 V vs. Na/Na^+ (Fig. S6), and prior work has shown an additional 0.2 V stability window when using tetraglyme-based electrolytes.[22] This presents an exciting range of options for high voltage anode-free sodium batteries with lower cost and competitive or enhanced energy density over current lithium-ion battery chemistries employing graphite host anodes. Such performance would not be possible with existing electrode configurations for Na-ion batteries employing host anode materials. Additionally, transitioning from vanadium to more abundant and environmentally-benign transition metals (iron and/or manganese) may be of interest, potentially through the use of Prussian white[9] or iron sulfates[10]. Furthermore, the use of high cathode areal loadings is a promising method to boost the cycle life and the energy density, as an increase in the plating capacity per unit area will reduce the first-cycle loss and improves the Coulombic efficiency of subsequent cycles. In regard to safety considerations, the stability of the sodium metal in the diglyme electrolyte and the capability to discharge the cell to a sodium metal-free state are an encouraging start. Future progress in this direction may include the development of non-flammable polymer electrolytes, advanced separators, and diagnostic tools adapted to this battery type. With the promising performance demonstrated and future research directions outlined in this work, the anode-free sodium battery is positioned to overcome the commercial challenges faced by SIBs and become an attractive alternative for stationary electric storage.

4. Experimental Section

Carbon-coated $Na_3V_2(PO_4)_3$ synthesis. V_2O_5, $NaH_2PO_4 \cdot H_2O$, and citric acid were combined in a molar ratio of 1:3:3 and then ball milled in ethanol in a planetary ball mill (FRITZ, Pulverisette 7) at 300 RPMs for 24 hours. The resulting green slurry was dried, hand ground using a mortar and pestle, and subsequently sintered at 350 ^oC in Ar for 4 hours. Afterwards, the powder was hand ground again using a mortar and pestle, pressed into 1 cm diameter discs, and sintered at 800 ^oC in Ar for 8 hours. Finally, the discs were ground into powder using a mortar and pestle and carbonized under Ar and C_2H_2 (90:10 volumetric flow ratio, respectively) for 30 minutes, while ramping from 600 ^oC to 690 ^oC.

Hard carbon synthesis. An aqueous sucrose solution (1.5 M) was kept at 190 ^oC in an autoclave for 5 hours, dried, and then pyrolyzed at 1100 ^oC under an Ar flow for 5 hours.

Characterization. SEM imaging was performed using a Zeiss MERLIN with GEMINI II SEM. XRD was performed using a Rigaku SmartLab XRD.

Electrochemical testing. Nucleation layers were made by mixing active material (70%) with TIMCAL Super C45 carbon black (10%) and CMC binder (20%) using water as the solvent. High-loading NVP electrodes were made using 80% active material, 5% CMC binder, 5% Polyolefin grafted acrylic acid copolymer, and 10% carbon black. These electrodes were processed with water:IPA (80:20 wt%). All slurries were spread onto carbon-coated Al foil (MTI) and then punched as 1 cm diameter discs and dried in a vacuum oven at 70 ^oC prior to device assembly. An electrolyte of 1M $NaPF_6$ in diglyme was used for all electrochemical testing. Prior to making electrolyte, $NaPF_6$ salt (Strem, 99%) was dried at 100 ^oC overnight in an Ar glovebox and diglyme (99.5%, Sigma-Aldrich) was dried using 4A molecular sieves. Electrolyte was used within a day of preparation. Half cells were assembled using sodium metal that was pressed flat onto a stainless steel disc, a Celgard 2325 separator, ~40 μl of electrolyte, and crimped in CR2032 coin cells. The results from Figure 2 and 3 were conducted using loadings of ~1 mg/cm^2. Anode-free cells were assembled using a 1 cm diameter nucleation layer disc, a Celgard 2325 separator, a Whatman glass fiber separator, and a 1 cm diameter cathode disc, ~100 μl of electrolyte, and crimped in CR2032 coin cells. All electrochemical testing was conducted using an MTI 8 Channel Battery Analyzer (0.005 – 1 mA).

Acknowledgements

The authors thank K. Hatzell for generous use of planetary ball mill, and M. Li, K. Moyer, A. Remirez, C. Klein, N. Robinson, F. Shen, K. Wolfe, and J. Eaves for helpful discussions. This work was supported in part by NSF CMMI grant 1400424, NSF Graduate Research Fellowships grant 1445197 awarded to A.P.C and K.S.

Conflicts of interest

There are no conflicts to declare.

Figure captions

Figure 1. (a) Schematic diagram illustrating the difference between the sodium-ion battery and the anode-free sodium battery. (b) Energy density comparison between battery configurations using different negative electrodes with a $Na_3V_2(PO_4)_3$ cathode; the anode-free approach using a nucleation layer is highlighted on the bottom.

Figure 2. (a,b) Electrochemical voltage profiles of the third cycle for sodium ion insertion/extraction at 0.1 A/g for carbon black (left) and hard carbon (right) electrodes. (c,d) Sodium metal nucleation profiles at 40 μA/cm^2 on sodiated electrodes. (e,f) Slippage profiles for sodium metal plating and stripping over 50 cycles at 0.5 mA/cm^2 on sodiated electrodes.

Figure 3. (a,b) Electrochemical voltage profiles of the third cycle for sodium ion alloying/dealloying at 0.1 A/g for bismuth (left) and tin (right) electrodes. (c,d) Sodium metal nucleation profiles at 40 μA/cm^2 on sodiated electrodes. (e,f) Slippage profiles for sodium metal plating and stripping over 50 cycles at 0.5 mA/cm^2 on sodiated electrodes.

Figure 4. First-cycle voltage profiles for (a) sodium-ion storage in hard carbon at 0.1 A/g and (b) sodium metal plating on a 0.25 mg/cm^2 carbon black electrode at 0.5 mA/cm^2 for a capacity of 2 mAh/cm^2.

Figure 5. (a) SEM image of $Na_3V_2(PO_4)_3$ particles and corresponding (b) XRD pattern. (c) Voltage profile for $Na_3V_2(PO_4)_3$ half cell at C/6 (where C=117 mA/g).

Figure 6. (a) Schematic of the charged and discharged state of the anode-free cell. (b) Slippage profile for the first 20 cycles of the anode-free cell. Inset, nucleation spike during charging.

Figure 7. (a) 100-cycle voltage profiles for anode-free cells at 0.50 mA/cm^2 (above) and 0.25 mA/cm^2 (below). (b) Corresponding cycling capacity retention with decay curves plotted for guidance.

Figure 8. Disassembled anode-free cells after 100+ cycles showing deposited sodium metal (charged state) for devices cycled at (a) 0.5 mA/cm^2 and (b) 0.25 mA/cm^2.

Figure 1.

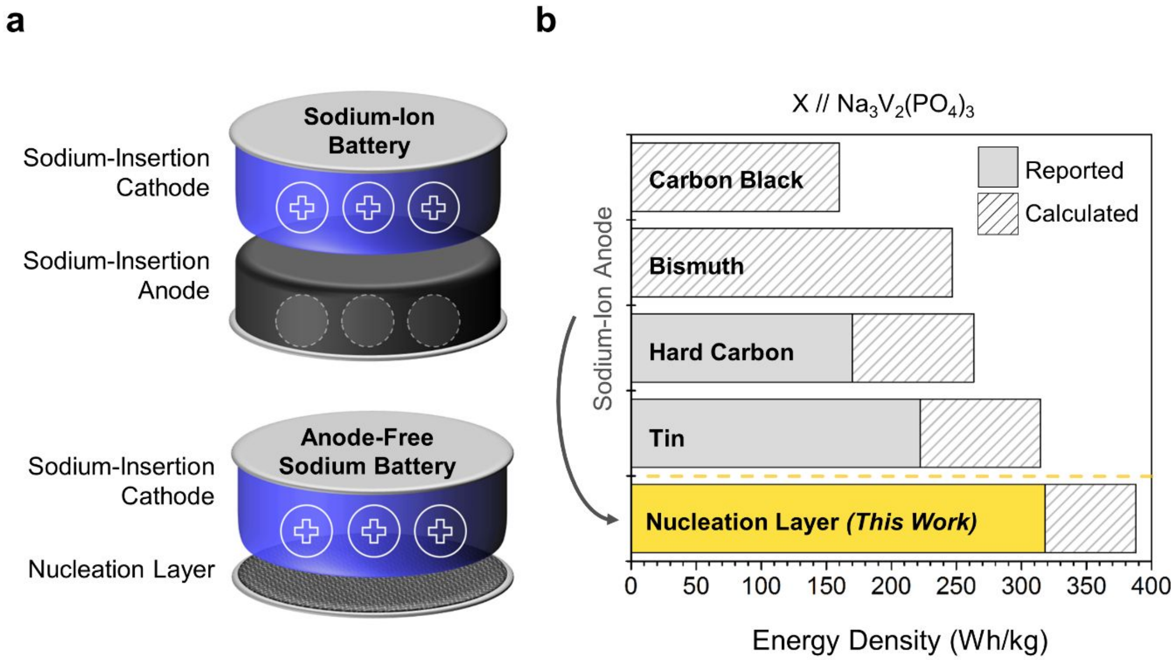
a
b
Sodium-Ion Battery
Sodium-Insertion Cathode
Sodium-Insertion Anode
Anode-Free Sodium Battery
Sodium-Insertion Cathode
Nucleation Layer
X // $Na_3V_2(PO_4)_3$
Reported
Calculated
Carbon Black
Bismuth
Hard Carbon
Tin
Nucleation Layer (This Work)
Sodium-Ion Anode
0
50
100
150
200
250
300
350
400
Energy Density (Wh/kg)

Figure 2.

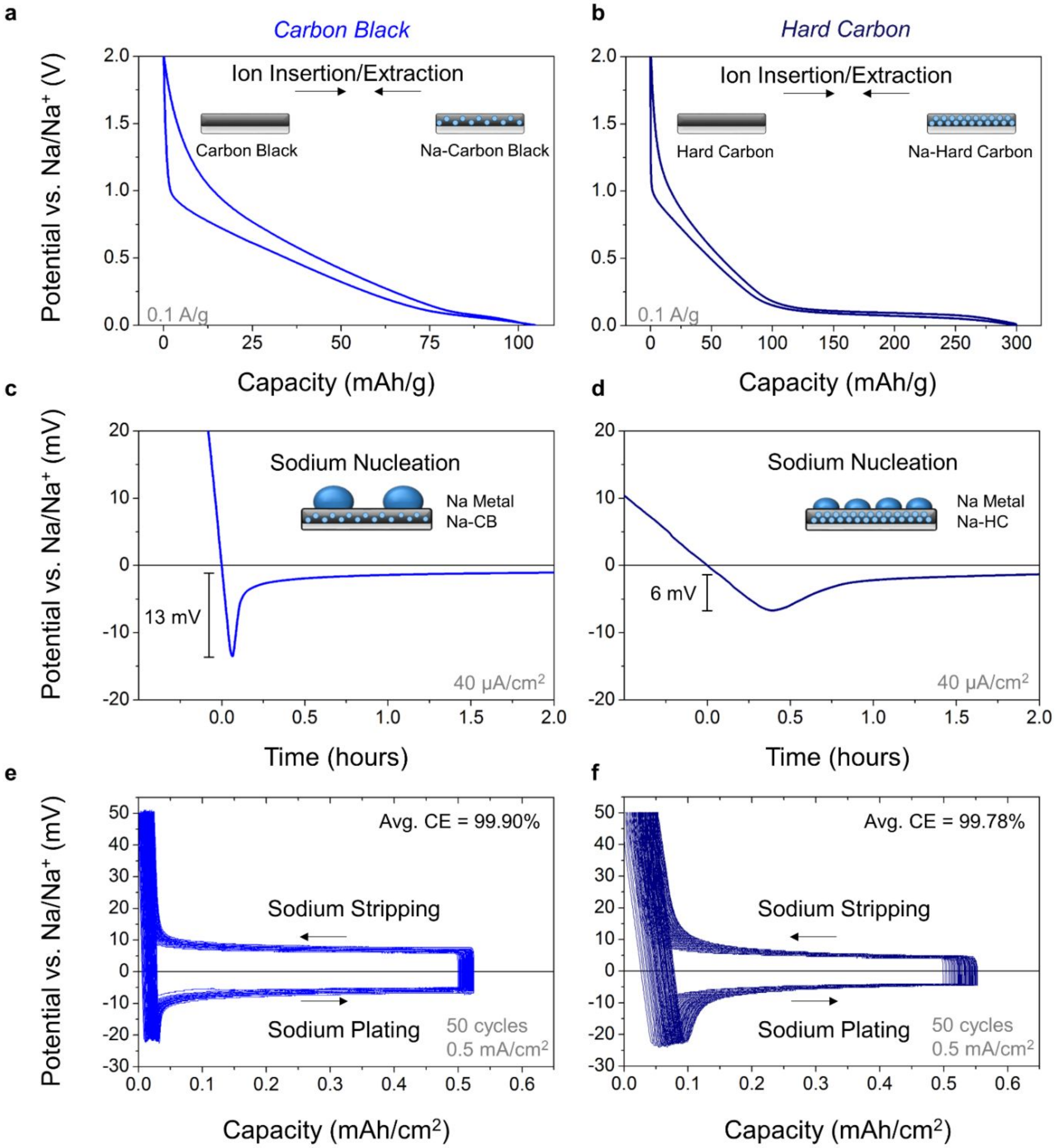
a
Carbon Black
Ion Insertion/Extraction
Carbon Black
Na-Carbon Black
0.1 A/g
Potential vs. Na/Na⁺ (V)
Capacity (mAh/g)
b
Hard Carbon
Ion Insertion/Extraction
Hard Carbon
Na-Hard Carbon
0.1 A/g
Capacity (mAh/g)
c
Sodium Nucleation
Na Metal
Na-CB
13 mV
40 μA/cm²
Potential vs. Na/Na⁺ (mV)
Time (hours)
d
Sodium Nucleation
Na Metal
Na-HC
6 mV
40 μA/cm²
Time (hours)
e
Avg. CE = 99.90%
Sodium Stripping
Sodium Plating
50 cycles
0.5 mA/cm²
Potential vs. Na/Na⁺ (mV)
Capacity (mAh/cm²)
f
Avg. CE = 99.78%
Sodium Stripping
Sodium Plating
50 cycles
0.5 mA/cm²
Capacity (mAh/cm²)

Figure 3.

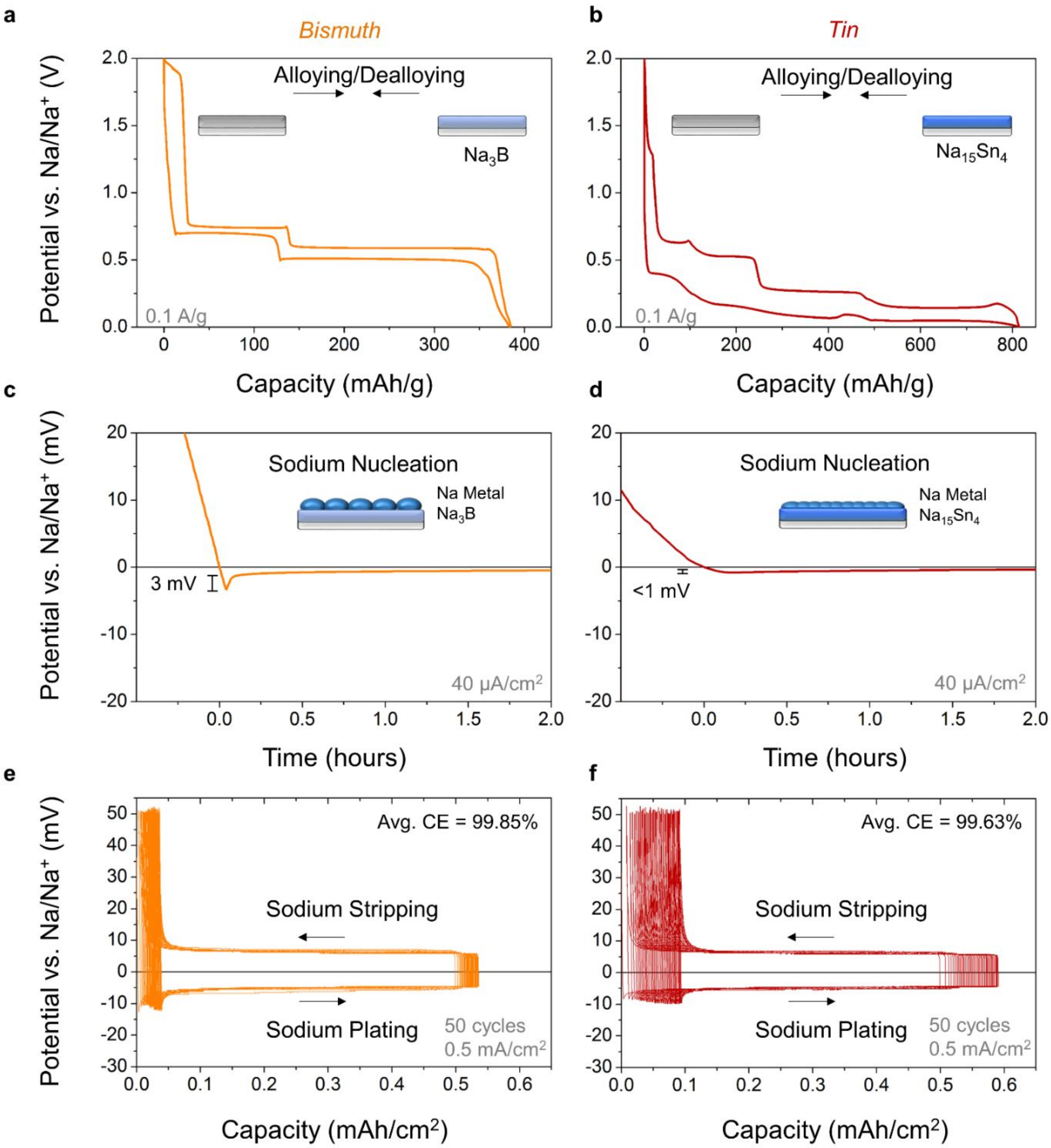
a
Bismuth
Alloying/Dealloying
Na3B
0.1 A/g
Potential vs. Na/Na+ (V)
Capacity (mAh/g)
b
Tin
Alloying/Dealloying
Na15Sn4
0.1 A/g
Capacity (mAh/g)
c
Sodium Nucleation
Na Metal
Na3B
3 mV
40 μA/cm2
Potential vs. Na/Na+ (mV)
Time (hours)
d
Sodium Nucleation
Na Metal
Na15Sn4
<1 mV
40 μA/cm2
Time (hours)
e
Avg. CE = 99.85%
Sodium Stripping
Sodium Plating
50 cycles
0.5 mA/cm2
Potential vs. Na/Na+ (mV)
Capacity (mAh/cm2)
f
Avg. CE = 99.63%
Sodium Stripping
Sodium Plating
50 cycles
0.5 mA/cm2
Capacity (mAh/cm2)

Figure 4.

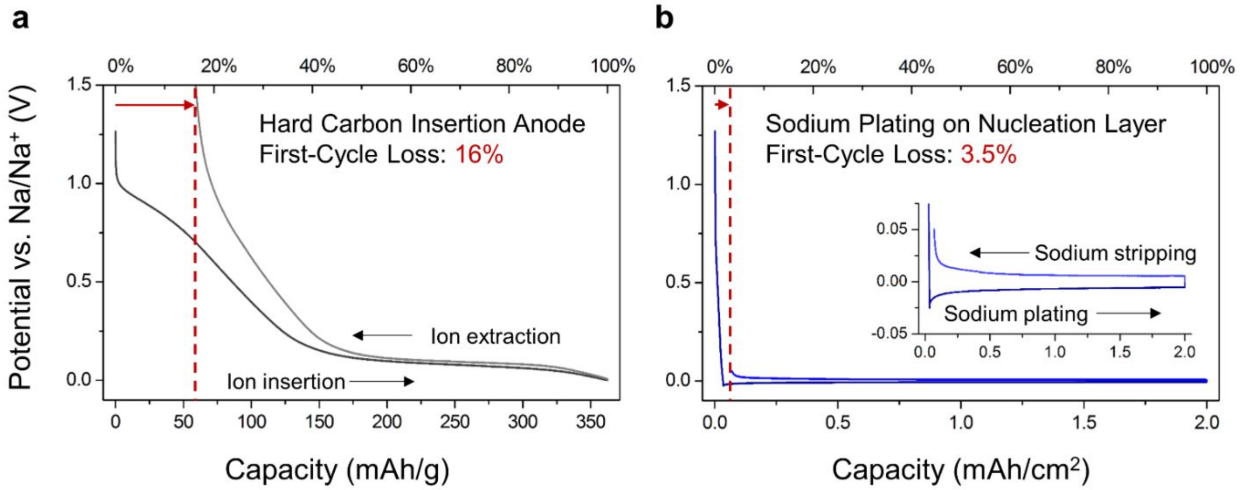
a
b
Hard Carbon Insertion Anode
First-Cycle Loss: 16%
Ion extraction
Ion insertion
Potential vs. Na/Na$^+$ (V)
Capacity (mAh/g)
0%
20%
40%
60%
80%
100%
1.5
1.0
0.5
0.0
0
50
100
150
200
250
300
350
Sodium Plating on Nucleation Layer
First-Cycle Loss: 3.5%
Sodium stripping
Sodium plating
0.05
0.00
-0.05
0.0
0.5
1.0
1.5
2.0
Capacity (mAh/cm^2)

Figure 5.

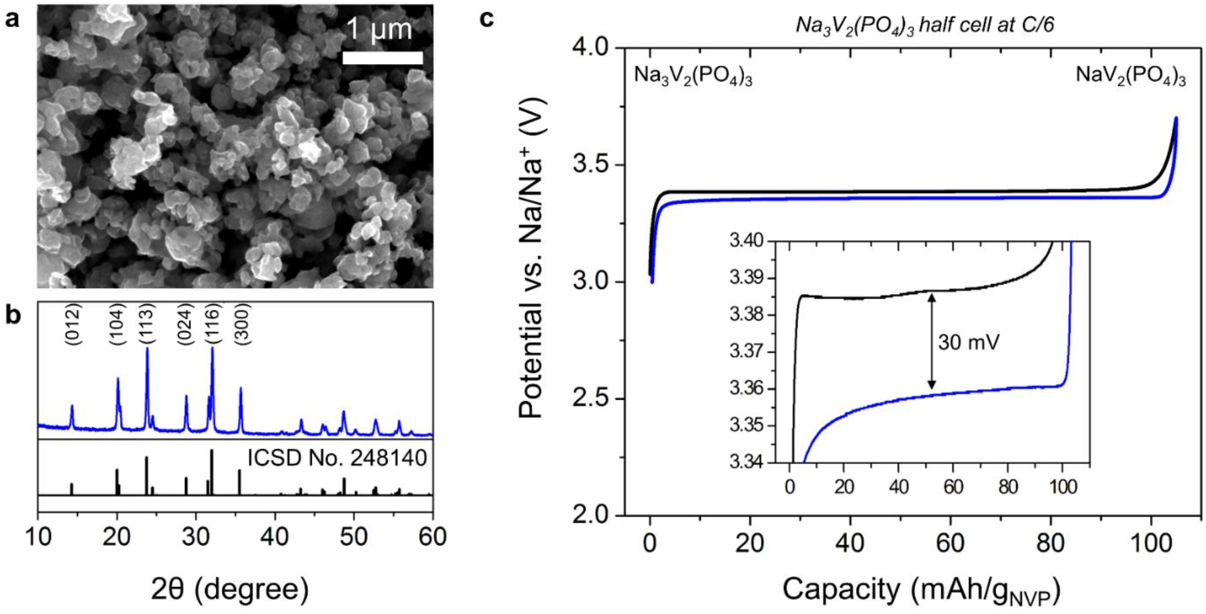
a
1 μm
b
(012)
(104)
(113)
(024)
(116)
(300)
ICSD No. 248140
10
20
30
40
50
60
2θ (degree)
c
$Na_3V_2(PO_4)_3$ half cell at C/6
$Na_3V_2(PO_4)_3$
$NaV_2(PO_4)_3$
Potential vs. Na/Na^+ (V)
4.0
3.5
3.0
2.5
2.0
0
20
40
60
80
100
Capacity (mAh/g_{NVP})
3.40
3.39
3.38
3.37
3.36
3.35
3.34
30 mV
0
20
40
60
80
100

Figure 6.

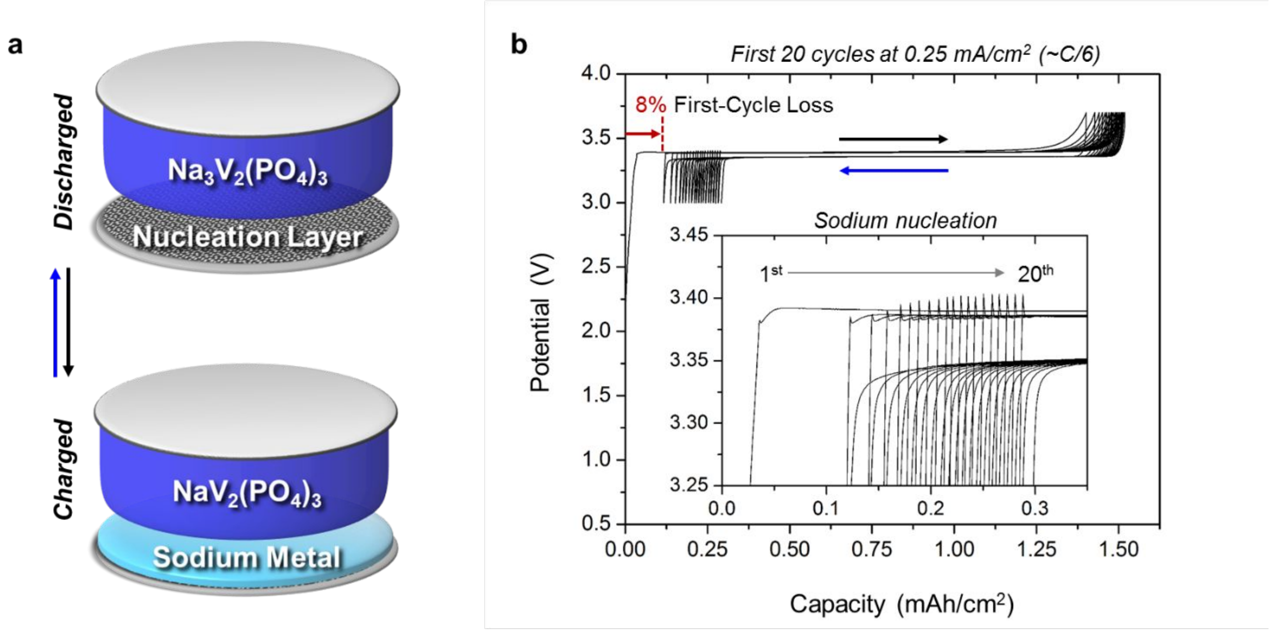
a
Discharged
Na3V2(PO4)3
Nucleation Layer
Charged
NaV2(PO4)3
Sodium Metal
b
First 20 cycles at 0.25 mA/cm2 (~C/6)
8% First-Cycle Loss
Sodium nucleation
1st
20th
Potential (V)
Capacity (mAh/cm2)
4.0
3.5
3.0
2.5
2.0
1.5
1.0
0.5
0.00
0.25
0.50
0.75
1.00
1.25
1.50
3.45
3.40
3.35
3.30
3.25
0.0
0.1
0.2
0.3

Figure 7.

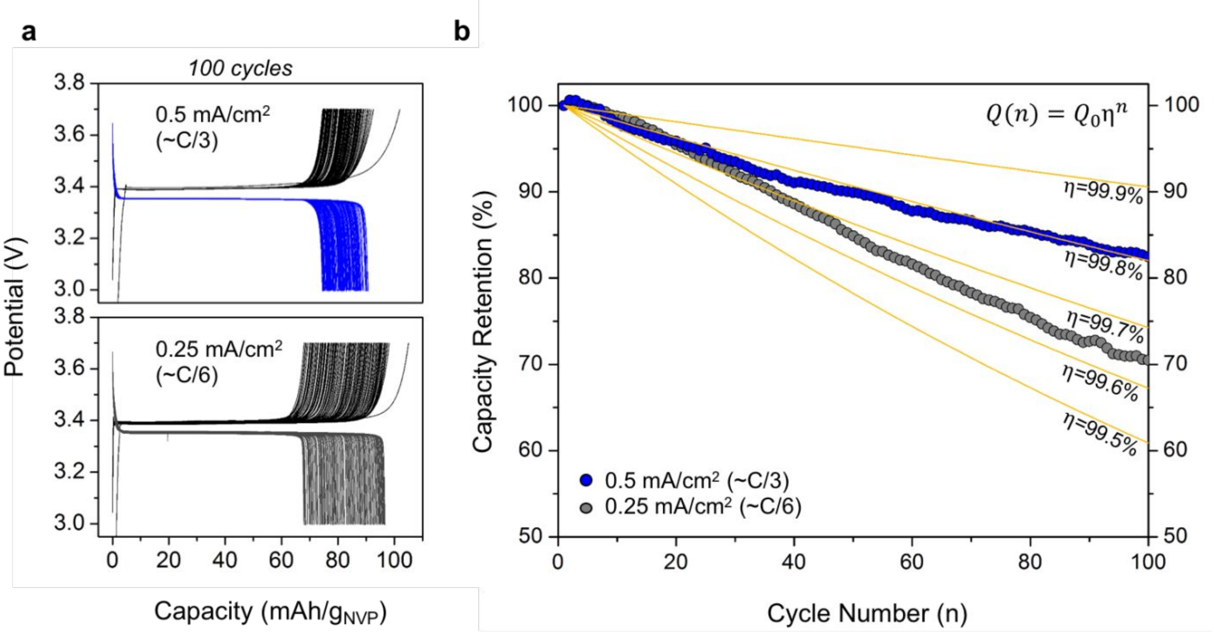
a
100 cycles
0.5 mA/cm²
(~C/3)
0.25 mA/cm²
(~C/6)
Potential (V)
3.0
3.2
3.4
3.6
3.8
0
20
40
60
80
100
Capacity (mAh/g$_{NVP}$)
b
$Q(n) = Q_0\eta^n$
η=99.9%
η=99.8%
η=99.7%
η=99.6%
η=99.5%
Capacity Retention (%)
50
60
70
80
90
100
● 0.5 mA/cm² (~C/3)
● 0.25 mA/cm² (~C/6)
Cycle Number (n)

Figure 8.

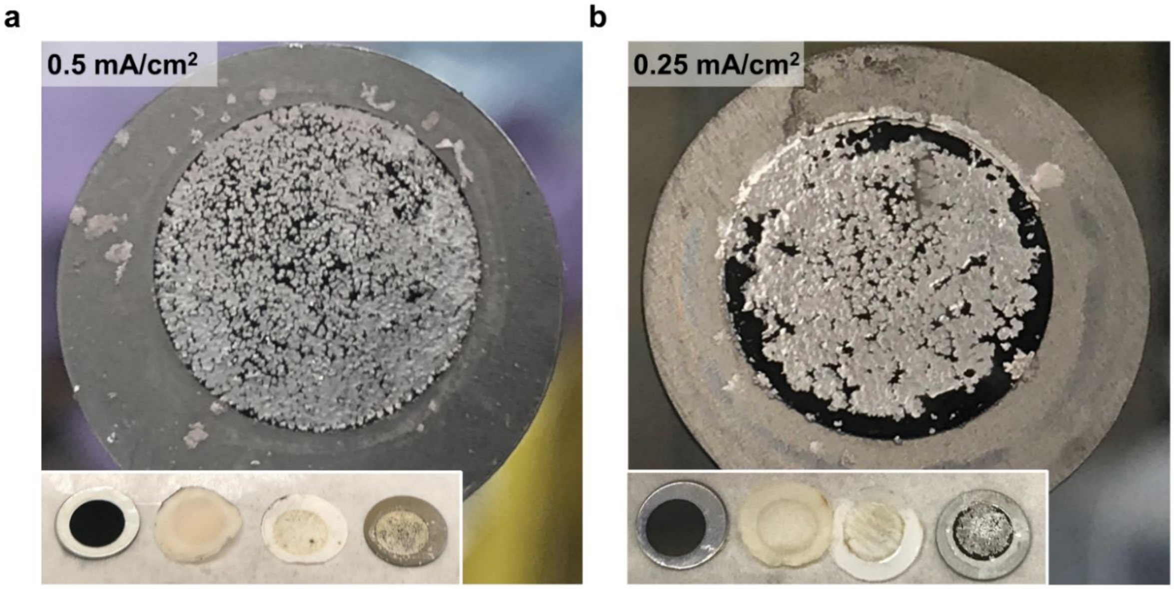

References

1. E. A. Olivetti, G. Ceder, G. G. Gaustad and X. Fu, *Joule*, 2017, **1**, 229-243.
2. Z. Li, M. S. Pan, L. Su, P.-C. Tsai, A. F. Badel, J. M. Valle, S. L. Eiler, K. Xiang, F. R. Brushett and Y.-M. Chiang, *Joule*, 2017, **1**, 306-327.
3. Y. Kim, K. H. Ha, S. M. Oh and K. T. Lee, *Chem. Eur. J*, 2014, **20**, 11980-11992.
4. J. W. Choi and D. Aurbach, *Nat. Rev. Mater.*, 2016, **1**, 16013.
5. N. Yabuuchi, M. Kajiyama, J. Iwatate, H. Nishikawa, S. Hitomi, R. Okuyama, R. Usui, Y. Yamada and S. Komaba, *Nat. Mater.*, 2012, **11**, 512-517.
6. M. H. Han, E. Gonzalo, G. Singh and T. Rojo, *Energy Environ. Sci.*, 2015, **8**, 81-102.
7. Y.-U. Park, D.-H. Seo, H.-S. Kwon, B. Kim, J. Kim, H. Kim, I. Kim, H.-I. Yoo and K. Kang, *J. Am. Chem. Soc.*, 2013, **135**, 13870-13878.
8. B. Ellis, W. Makahnouk, Y. Makimura, K. Toghill and L. Nazar, *Nat. Mater.*, 2007, **6**, 749-753.
9. L. Wang, J. Song, R. Qiao, L. A. Wray, M. A. Hossain, Y.-D. Chuang, W. Yang, Y. Lu, D. Evans, J.-J. Lee, V. Sean, X. Zhao, M. Nishijima, S. Kakimoto and J. B. Goodenough, *J. Am. Chem. Soc.*, 2015, **137**, 2548-2554.
10. P. Barpanda, G. Oyama, S.-i. Nishimura, S.-C. Chung and A. Yamada, *Nat. Commun.*, 2014, **5**, 4358.
11. Z. Jian, L. Zhao, H. Pan, Y.-S. Hu, H. Li, W. Chen and L. Chen, *Electrochem. Commun.*, 2012, **14**, 86-89.
12. Y. Liu, B. V. Merinov and W. A. Goddard, *Natl. Acad. Sci. U.S.A.*, 2016, **113**, 3735-3739.
13. M. D. Slater, D. Kim, E. Lee and C. S. Johnson, *Adv. Funct. Mater.*, 2013, **23**, 947-958.
14. D. Stevens and J. Dahn, *J. Electrochem. Soc.*, 2000, **147**, 1271-1273.
15. E. Irisarri, A. Ponrouch and M. Palacin, *J. Electrochem. Soc.*, 2015, **162**, A2476-A2482.
16. J. Zhang, D.-W. Wang, W. Lv, S. Zhang, Q. Liang, D. Zheng, F. Kang and Q.-H. Yang, *Energy Environ. Sci.*, 2017, **10**, 370-376.
17. Y.-E. Zhu, L. Yang, X. Zhou, F. Li, J. Wei and Z. Zhou, *J. Mater. Chem. A*, 2017, **5**, 9528-9532.
18. B. Jache and P. Adelhelm, *Angew. Chem. Int. Ed.*, 2014, **53**, 10169-10173.
19. A. P. Cohn, K. Share, R. Carter, L. Oakes and C. L. Pint, *Nano Lett.*, 2015, **16**, 543-548.
20. B. Zhang, G. Rousse, D. Foix, R. Dugas, D. A. D. Corte and J. M. Tarascon, *Adv. Mater.*, 2016, **28**, 9824-9830.
21. C. Wang, L. Wang, F. Li, F. Cheng and J. Chen, *Adv. Mater.*, 2017, **29**, 1702212.
22. Z. W. Seh, J. Sun, Y. Sun and Y. Cui, *ACS Cent. Sci.*, 2015, **1**, 449-455.
23. V. Etacheri, R. Marom, R. Elazari, G. Salitra and D. Aurbach, *Energy Environ. Sci.*, 2011, **4**, 3243-3262.
24. A. Wang, X. Hu, H. Tang, C. Zhang, S. Liu, Y. Yang, Q. Yang and J. Luo, *Angew. Chem.*, 2017, **129**, 12083.
25. B. Neudecker, N. Dudney and J. Bates, *J. Electrochem. Soc.*, 2000, **147**, 517-523.
26. J. Qian, B. D. Adams, J. Zheng, W. Xu, W. A. Henderson, J. Wang, M. E. Bowden, S. Xu, J. Hu and J. G. Zhang, *Adv. Funct. Mater.*, 2016, **26**, 7094-7102.
27. A. P. Cohn, N. Muralidharan, R. Carter, K. Share and C. L. Pint, *Nano Lett.*, 2017, **17**, 1296-1301.
28. C. Vaalma, D. Buchholz, M. Weil and S. Passerini, *Nat. Rev. Mater.*, 2018, **3**, 18013.
29. C. Bommier, T. W. Surta, M. Dolgos and X. Ji, *Nano Lett.*, 2015, **15**, 5888-5892.

30. K. Yan, Z. Lu, H.-W. Lee, F. Xiong, P.-C. Hsu, Y. Li, J. Zhao, S. Chu and Y. Cui, *Nat. Energy*, 2016, **1**, 16010.
31. T. Ohzuku, Y. Iwakoshi and K. Sawai, *J. Electrochem. Soc.*, 1993, **140**, 2490-2498.
32. A. Pei, G. Zheng, F. Shi, Y. Li and Y. Cui, *Nano Lett.*, 2017, **17**, 1132-1139.
33. N. N. Sinha, A. Smith, J. C. Burns, G. Jain, K. Eberman, E. Scott, J. Gardner and J. Dahn, *J. Electrochem. Soc.*, 2011, **158**, A1194-A1201.
34. R. Zhang, X. R. Chen, X. Chen, X. B. Cheng, X. Q. Zhang, C. Yan and Q. Zhang, *Angew. Chem. Int. Ed.*, 2017, **56**, 7764.
35. C. Yang, Y. Yao, S. He, H. Xie, E. Hitz and L. Hu, *Adv. Mater.*, 2017, **29**, 1702714.
36. L. Medenbach, C. L. Bender, R. Haas, B. Mogwitz, C. Pompe, P. Adelhelm, D. Schröder and J. Janek, *Energy Technol.*, 2017, **5**, 2265.
37. V. Aravindan, Y. S. Lee and S. Madhavi, *Adv. Energy Mater.*, 2017, **7**, 1602607.
38. B. Zhang, R. Dugas, G. Rousse, P. Rozier, A. M. Abakumov and J.-M. Tarascon, *Nat. Commun.*, 2016, **7**, 10308.
39. R. Klee, M. J. Aragón, R. Alcántara, J. L. Tirado and P. Lavela, *Eur. J. Inorg. Chem.*, 2016, **2016**, 3212-3218.
40. Z. Du, K. Rollag, J. Li, S. An, M. Wood, Y. Sheng, P. Mukherjee, C. Daniel and D. Wood, *J. Power Sources*, 2017, **354**, 200-206.
41. A. Smith, H. M. Dahn, J. Burns and J. Dahn, *J. Electrochem. Soc.*, 2012, **159**, A705-A710.
42. J. Cannarella and C. B. Arnold, *J. Power Sources*, 2014, **245**, 745-751.
43. C. J. Bae, C. K. Erdonmez, J. W. Halloran and Y. M. Chiang, *Adv. Mater.*, 2013, **25**, 1254-1258.
44. P. Meister, H. Jia, J. Li, R. Kloepsch, M. Winter and T. Placke, *Chem. Mater.*, 2016, **28**, 7203-7217.
45. J.-Y. Hwang, S.-M. Oh, S.-T. Myung, K. Y. Chung, I. Belharouak and Y.-K. Sun, *Nat. Commun.*, 2015, **6**, 6865.

TOC Image

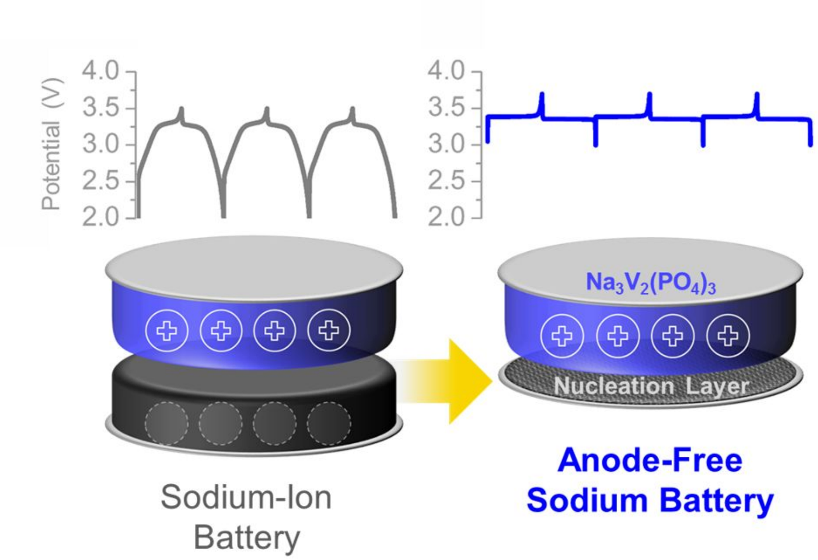

The anode-free sodium battery with a nucleation layer is presented as a low-cost, high-performance option for stationary electric storage.

Electronic Supplementary Information

Rethinking Sodium-Ion Anodes as Nucleation Layers for Anode-Free Batteries

Adam P. Cohn[1], Thomas Metke[1], Jennifer Donohue[1], Nitin Muralidharan[2] , Keith Share[2], and Cary L. Pint[1,2]*

[1]Department of Mechanical Engineering, Vanderbilt University, Nashville, TN 37235

[2]Interdisciplinary Materials Science Program, Vanderbilt University, Nashville, TN 37235

Table 1. Specific capacity and average voltage values used to calculate full-cell energy densities

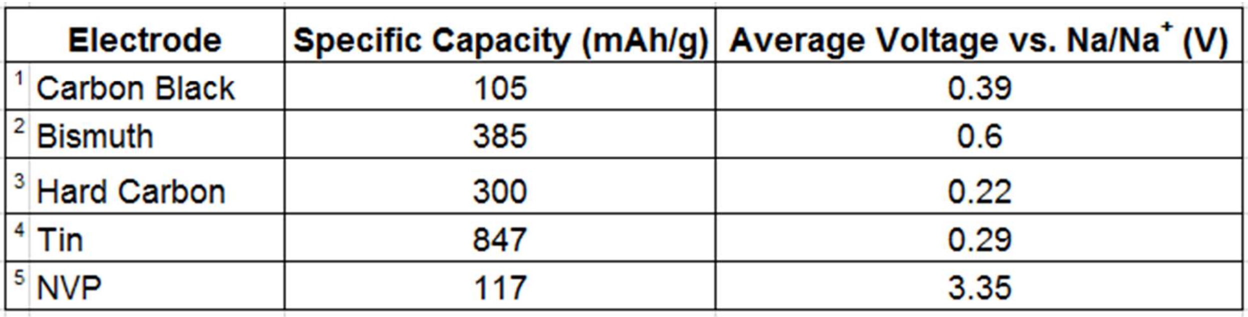

Electrode	Specific Capacity (mAh/g)	Average Voltage vs. Na/Na$^+$ (V)
[1] Carbon Black	105	0.39
[2] Bismuth	385	0.6
[3] Hard Carbon	300	0.22
[4] Tin	847	0.29
[5] NVP	117	3.35

1. Carbon black specific capacity and average extraction voltage were determined from half cell testing at 0.1 A/g, as shown in Figure 2a.
2. Bismuth specific capacity was calculated with respect to the final alloy Na_3B. The average extraction voltage were determined from half cell testing at 0.1 A/g, as shown in Figure 3a.
3. Hard carbon specific capacity and average extraction voltage were determined from half cell testing at 0.1 A/g, as shown in Figure 2b.
4. Tin specific capacity was calculated with respect to the final alloy $Na_{15}Sn_4$. The average extraction voltage were determined from half cell testing at 0.1 A/g , as shown in Figure 3b.
5. NVP specific capacity was calculated with respect to the removal of two Na ions from $Na_3V_2(PO_4)_3$. The average insertion voltage were determined from half cell testing at 0.04 A/g.

Table 2. Volumetric energy density calculations for a cell with a loading of 2.5 mAh/cm^2

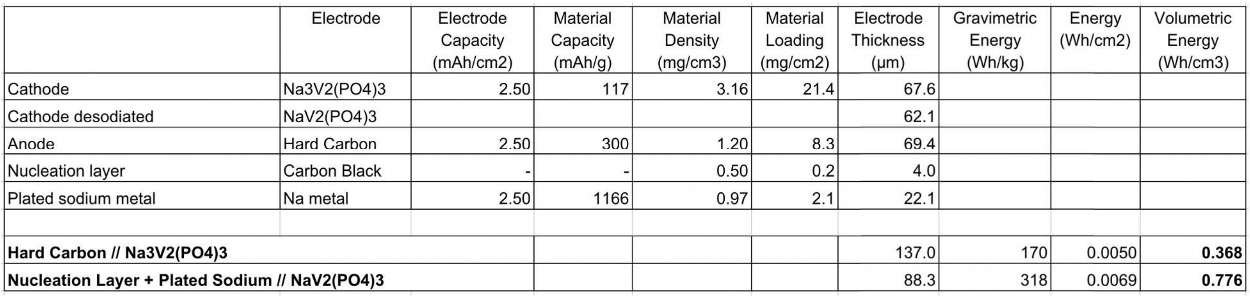

	Electrode	Electrode Capacity (mAh/cm2)	Material Capacity (mAh/g)	Material Density (mg/cm3)	Material Loading (mg/cm2)	Electrode Thickness (µm)	Gravimetric Energy (Wh/kg)	Energy (Wh/cm2)	Volumetric Energy (Wh/cm3)
Cathode	Na3V2(PO4)3	2.50	117	3.16	21.4	67.6			
Cathode desodiated	NaV2(PO4)3					62.1			
Anode	Hard Carbon	2.50	300	1.20	8.3	69.4			
Nucleation layer	Carbon Black	-	-	0.50	0.2	4.0			
Plated sodium metal	Na metal	2.50	1166	0.97	2.1	22.1			
Hard Carbon // Na3V2(PO4)3						137.0	170	0.0050	**0.368**
Nucleation Layer + Plated Sodium // NaV2(PO4)3						88.3	318	0.0069	**0.776**

For simplicity, only the active materials are considered. Current collectors, binders, separators, packaging, and electrode porosity are not considered. The hard carbon//NVP gravimetric energy density is taken from Ref. 20 and the hard carbon density is taken from Ref. 4.

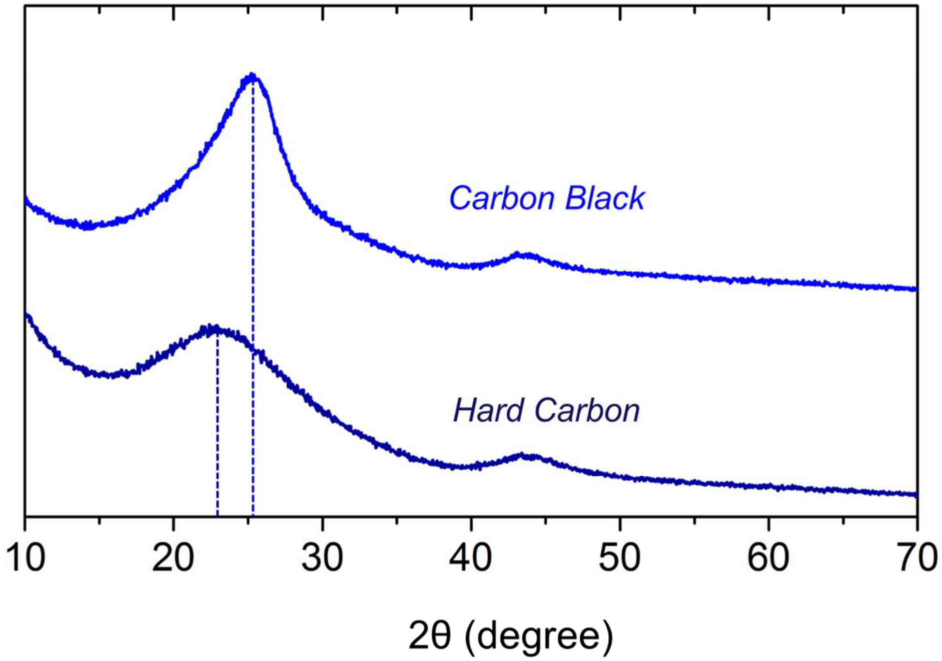

Figure S1. X-ray diffraction patterns for carbon black (TIMCAL Super C45) and synthesized hard carbon. The lower angle 002 peak (highlighted with the dashed line) observed for hard carbon indicates a larger interlayer spacing between graphene sheets in the hard carbon than the carbon black.

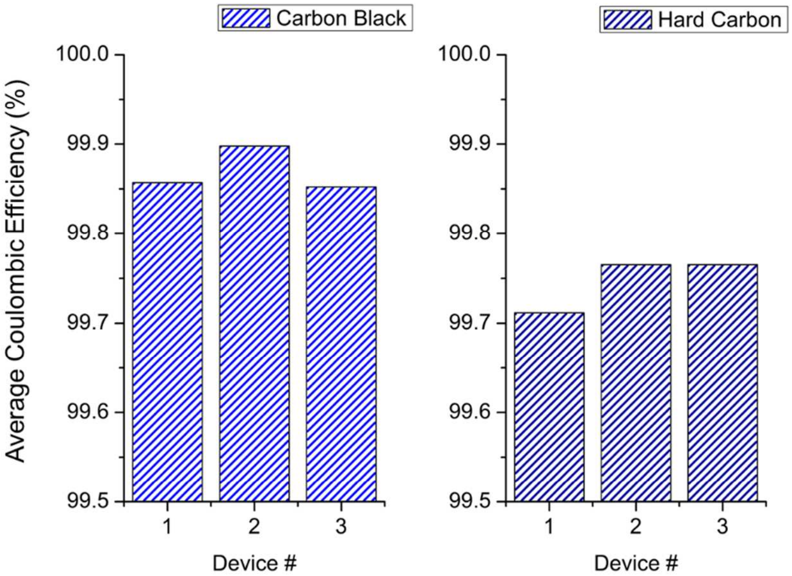

Figure S2. Average Coulombic efficiency over 50 cycles of plating and stripping of 0.5 mAh/cm^2 of sodium metal at a current of 0.5 mA/cm^2 for three carbon black devices (left) and three hard carbon devices (right). To minimize variation due to electrolyte or glovebox conditions, fresh electrolyte was always prepared prior to assembling cells, and batches of comparative cells were always made together (rather than making carbon black cells one day and hard carbon cells another day).

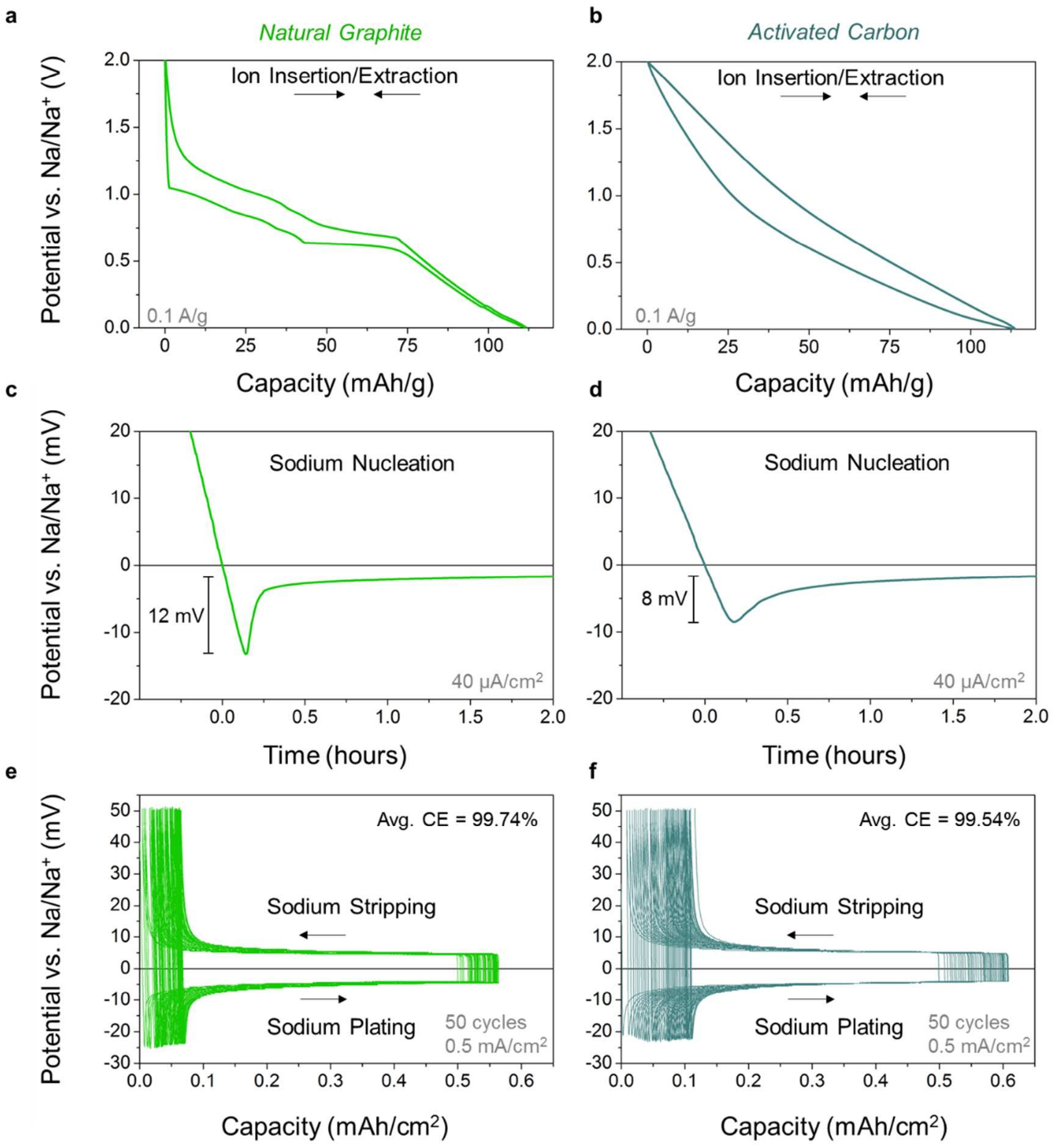

Figure S3. (a,b) Electrochemical voltage profiles of the third cycle for sodium ion insertion/extraction at 0.1 A/g for natural graphite (left) and activated carbon (right) electrodes. (c,d) Sodium metal nucleation profiles at 40 μA/cm^2 on sodiated electrodes. (e,f) Slippage profiles for sodium metal plating and stripping over 50 cycles at 0.5 mA/cm^2 on sodiated electrodes. For the natural graphite electrode, the process by which sodium ions insertion occurs is through the co-intercalation of sodium ions and diglyme molecules as detailed in Ref 18.

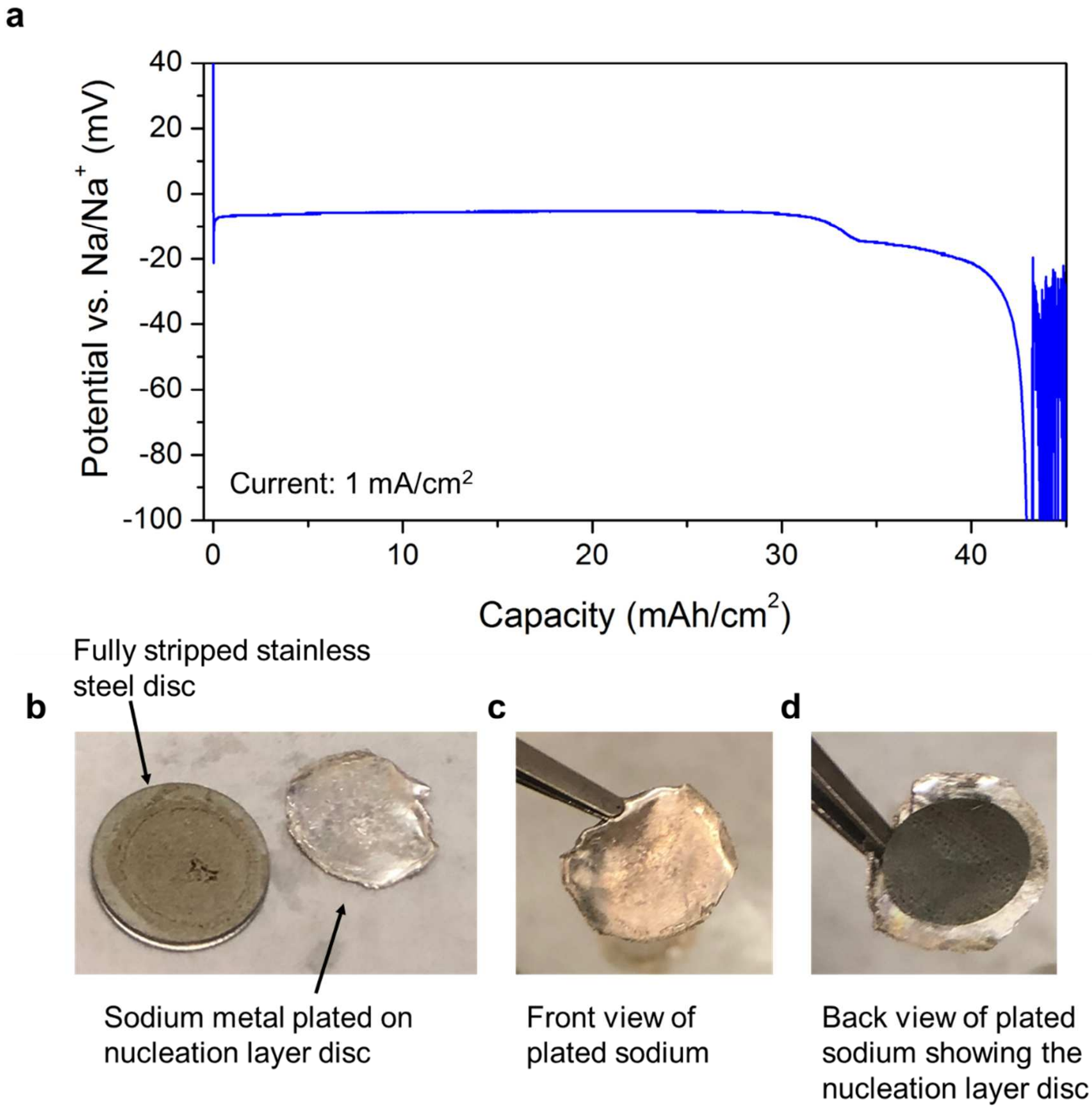

Figure S4. Plating on carbon black nucleation layer in a half-cell configuration until exhaustion of the sodium metal counter/reference electrode. Voltage profile shows stable plating over ~30 mAh/cm^2 of operation. Images show the full removal of all the sodium metal from the stainless steel disc and the deposition of sodium metal on the nucleation layer disc.

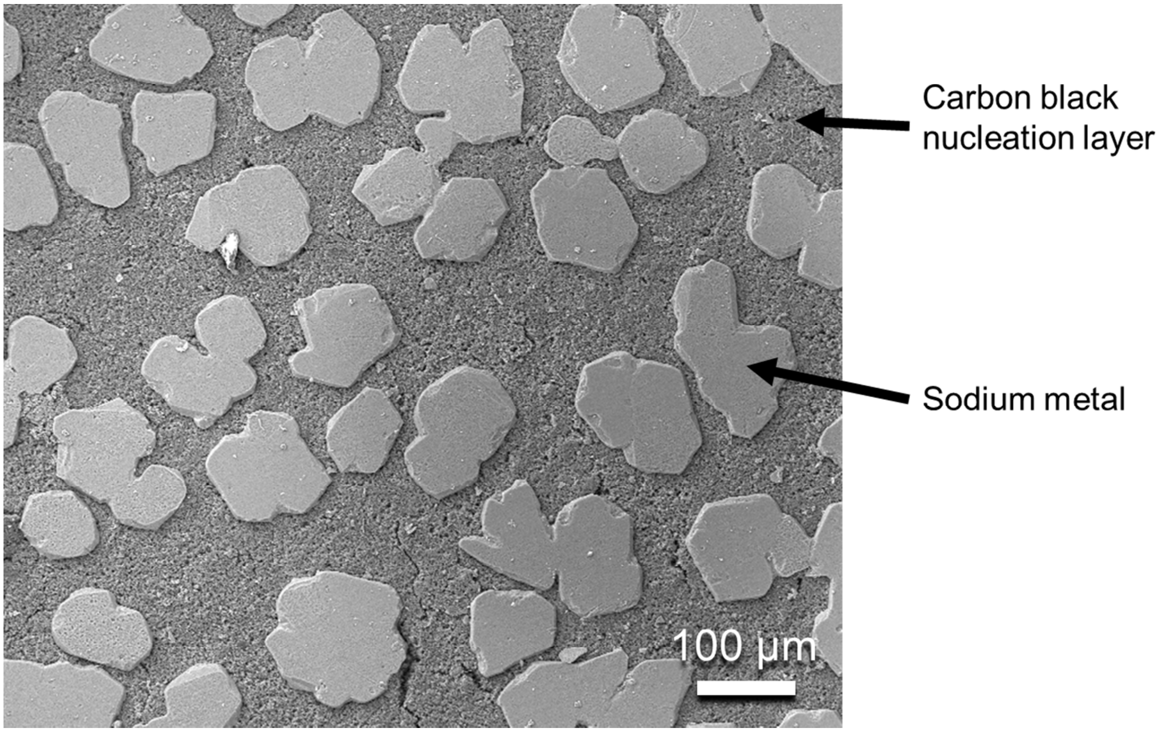

Figure S5. Scanning electron microscope image of sodium metal (0.5 mAh/cm^2) plated on a carbon black nucleation layer, showing the islands of sodium metal that appear to grow on the surface of the carbon black nucleation layer.

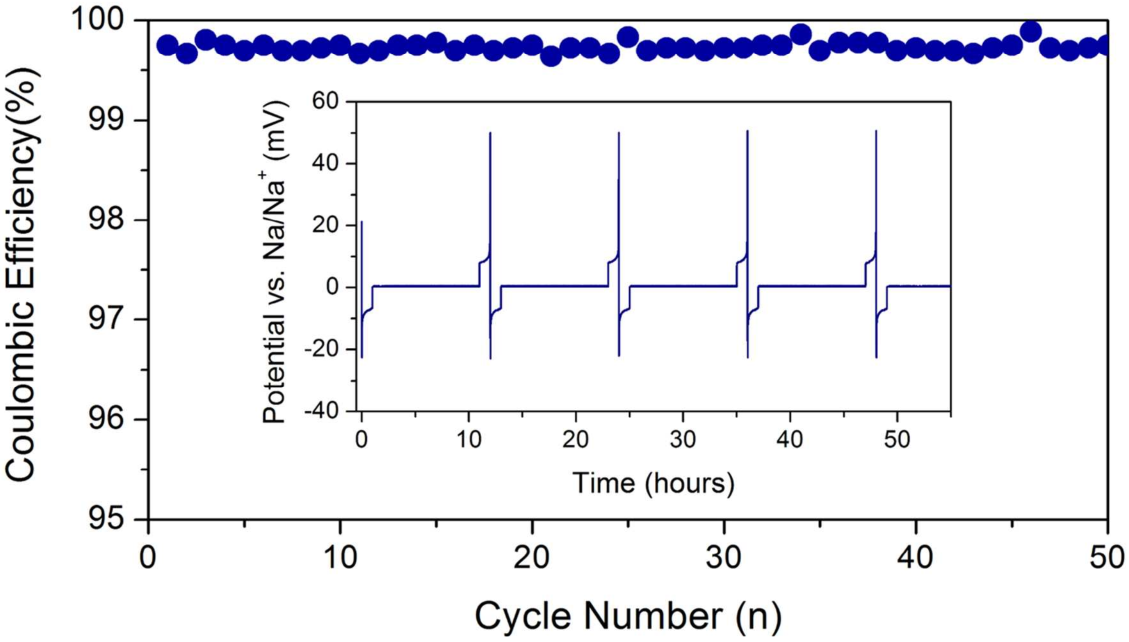

Current: 1 mA/cm^2
Capacity: 1 mAh/cm^2
Rest Period: 10 hours

Figure S6. 50 cycles of plating and stripping on a carbon black nucleation layer in a half-cell configuration using a 10 hour rest between each plating and stripping step to test the resting stability of the plated sodium metal. The inset shows the voltage profile for 4+ of these cycles. The average Coulombic efficiency of 99.73% over these 50 cycles indicates that minimal sodium is lost during the 10 hour resting period.

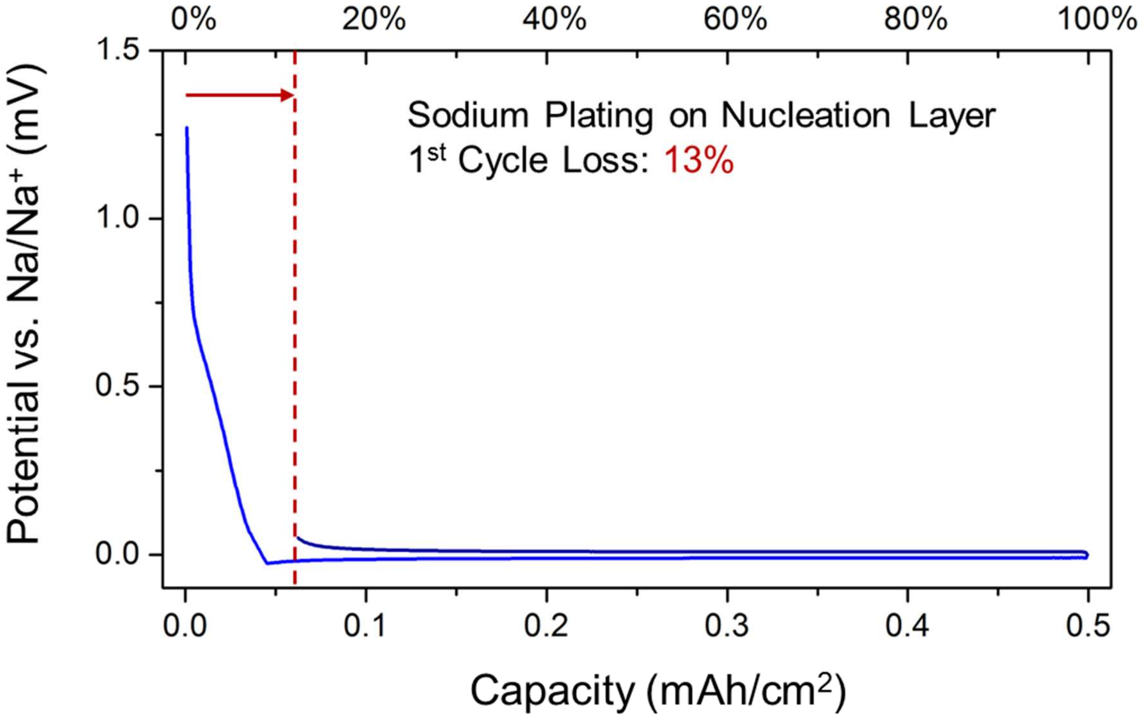

Figure S7. First-cycle voltage profiles for sodium metal plating on a 0.25 mg/cm^2 carbon black electrode at 0.5 mA/cm^2 for a capacity of 0.5 mAh/cm^2.

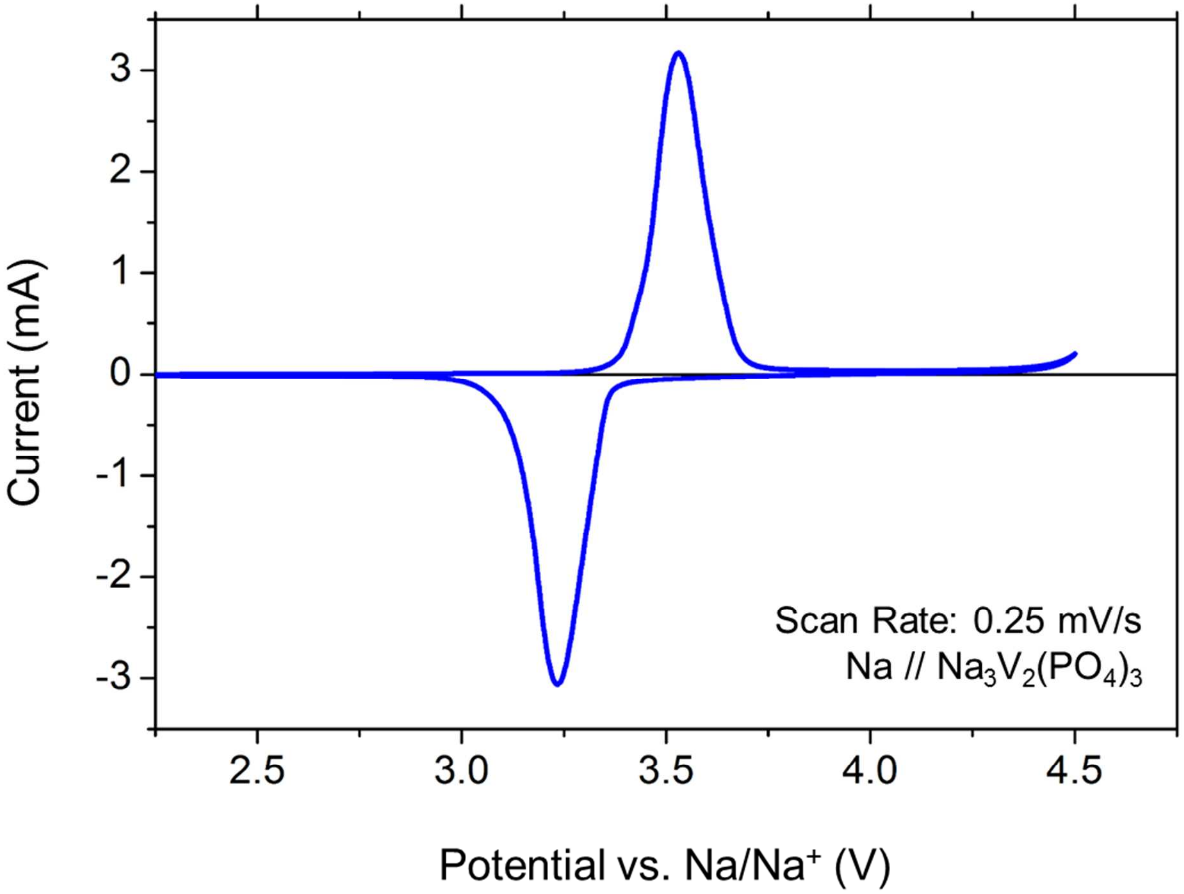

Figure S8. Cyclic voltammogram of $Na_3V_2(PO_4)_3$ half cell performed at 0.25 mV/s to 4.5 V vs. Na/Na^+ using an electrolyte of 1M $NaPF_6$ in diglyme. This test shows the electrochemical window of the 1M $NaPF_6$ in diglyme. To extend the electrochemical window of gylme-based electrolytes beyond what is shown here for 1M $NaPF_6$ in diglyme, the replacement of diglyme with tetraglyme[1] and the use of higher salt concentrations[2] can be carried out. Such electrolyte modifications should provide improved stability for the use of higher voltage cathodes.

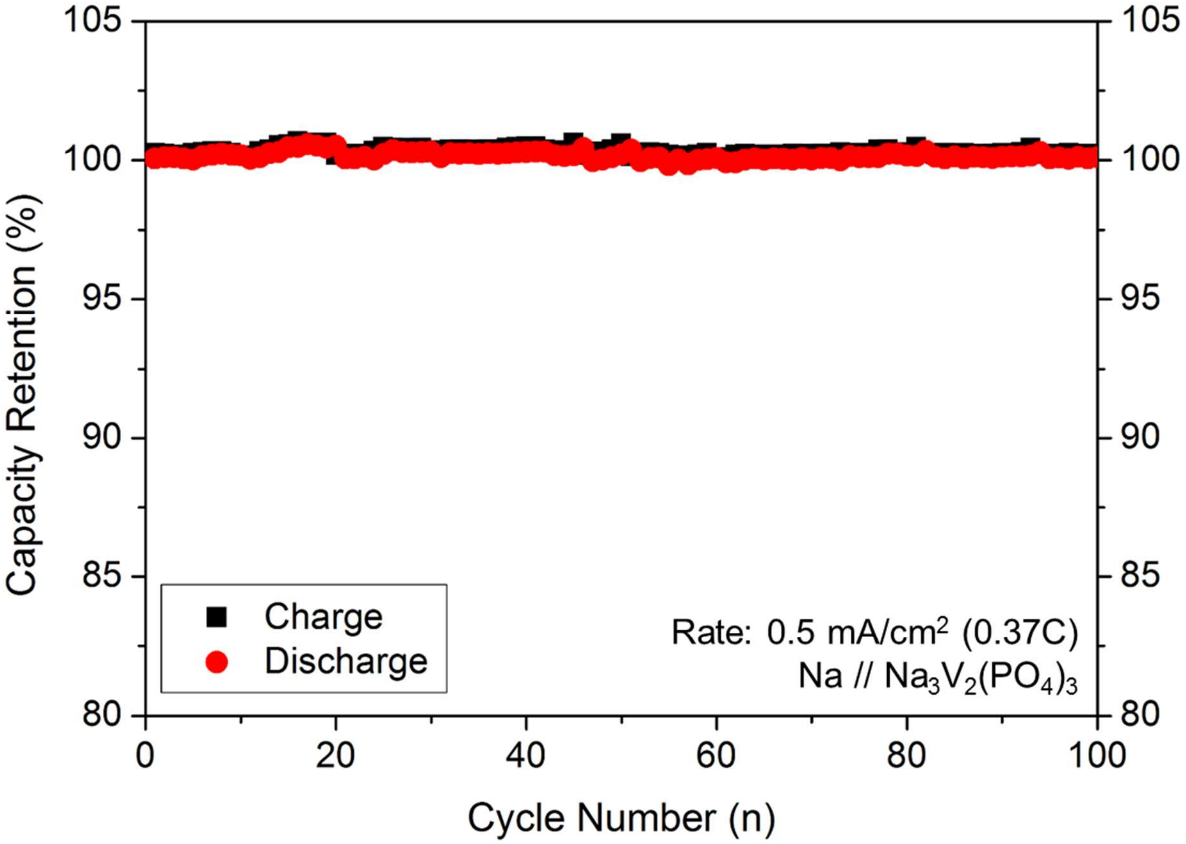

Figure S9. Cycling of $Na_3V_2(PO_4)_3$ in a half-cell configuration performed at 0.5 mA/cm^2 (0.37C) for 100 cycles.

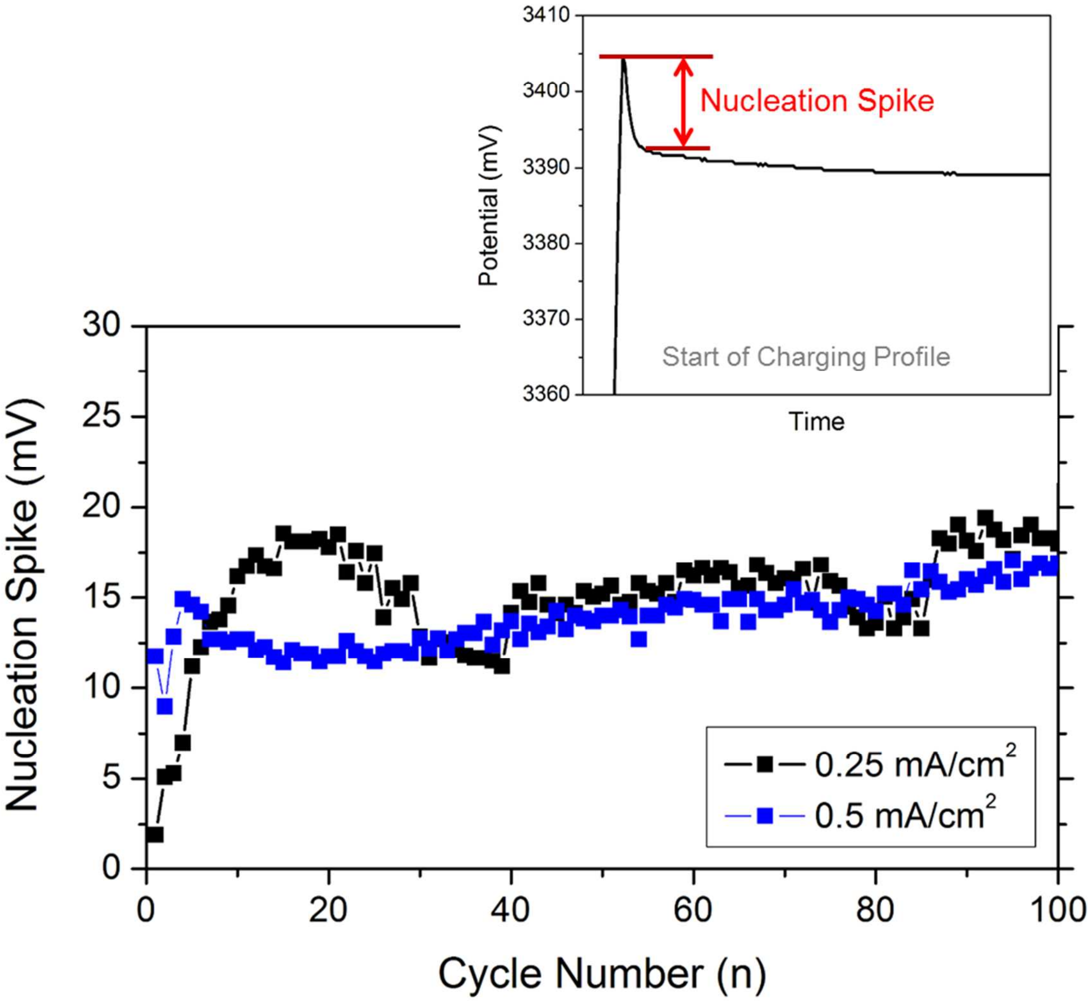

Figure S10. Nucleation spike voltage for anode-free cells cycled at 0.25 mA/cm^2 and 0.5 mA/cm^2. Above the panel is an example plot of the nucleation spike measurement. The slow loss of sodium in the cell causes the alignment of the cathode plateau and the nucleation events to slowly shift with cycle number. Whereas this can explain the initial change in the nucleation spike, the gradual increase over longer cycles could be related to more subtle changes at interfaces during cycling of the full cell device. Such a gradual increase in the spike magnitude was not observed in half-cell testing with carbon black nucleation layers.

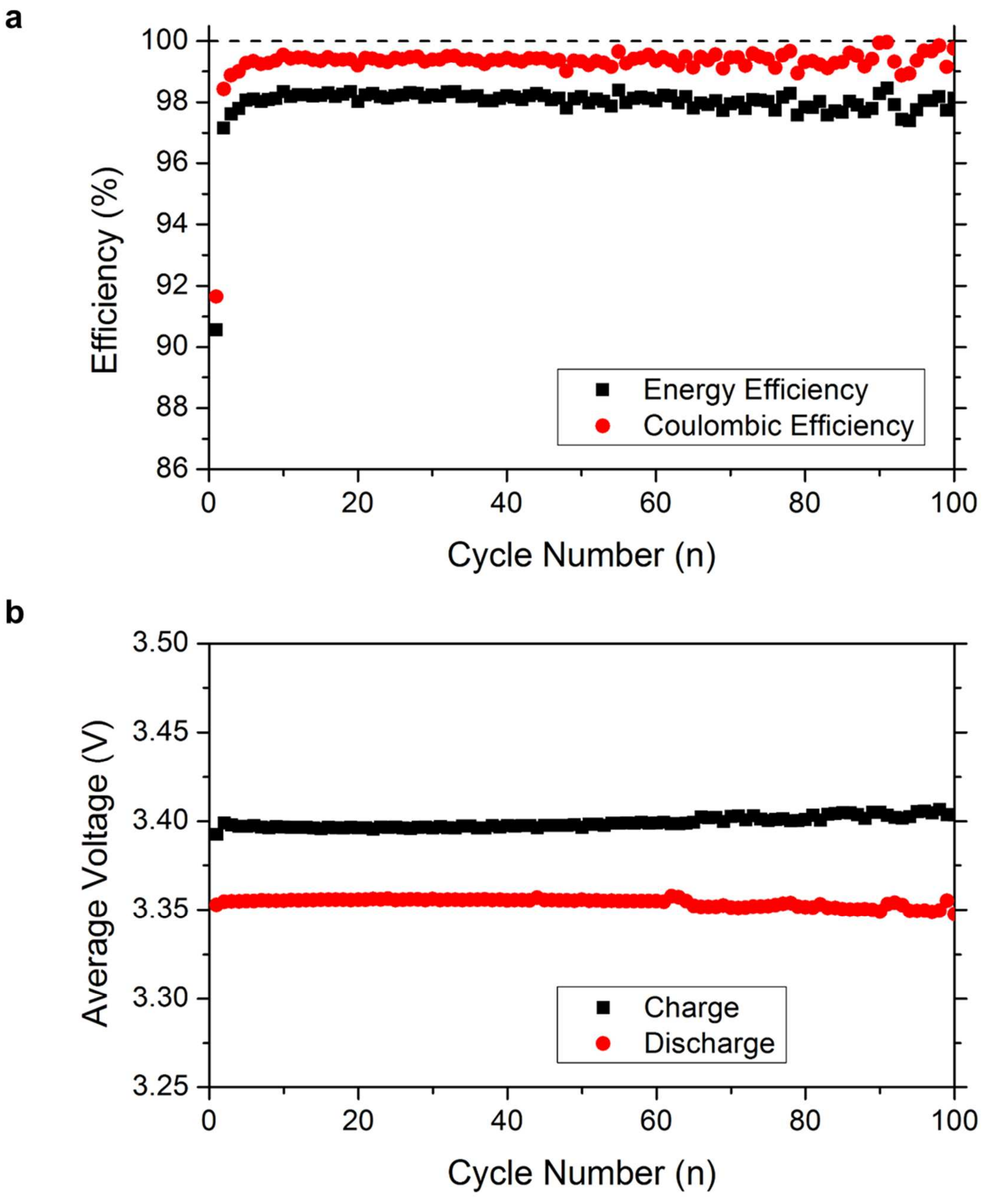

Figure S11. (a) Cycling efficiency and (b) average voltage for anode-free cell cycled at 0.25 mA/cm^2.

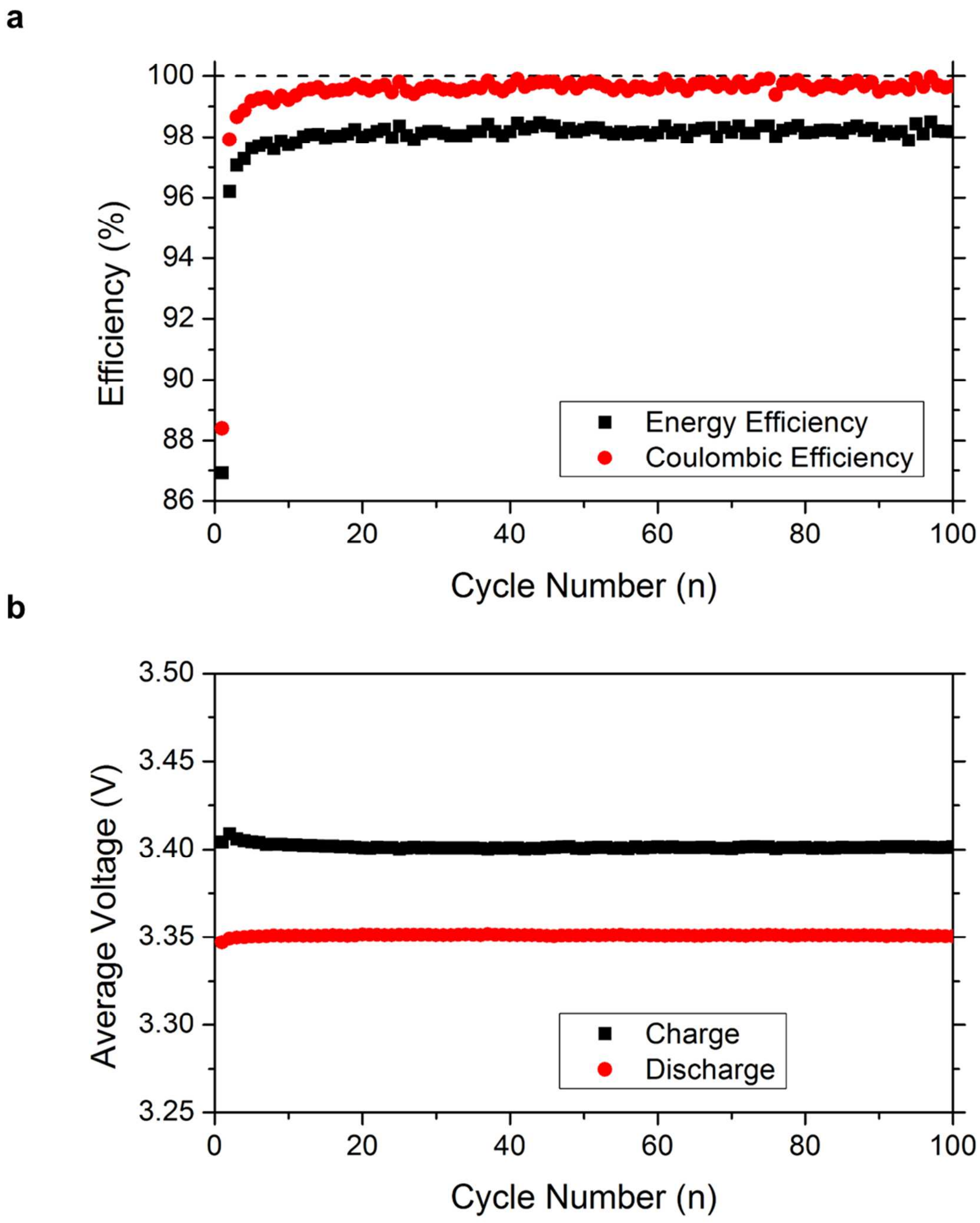

Figure S12. (a) Cycling efficiency and (b) average voltage for anode-free cell cycled at 0.5 mA/cm^2.

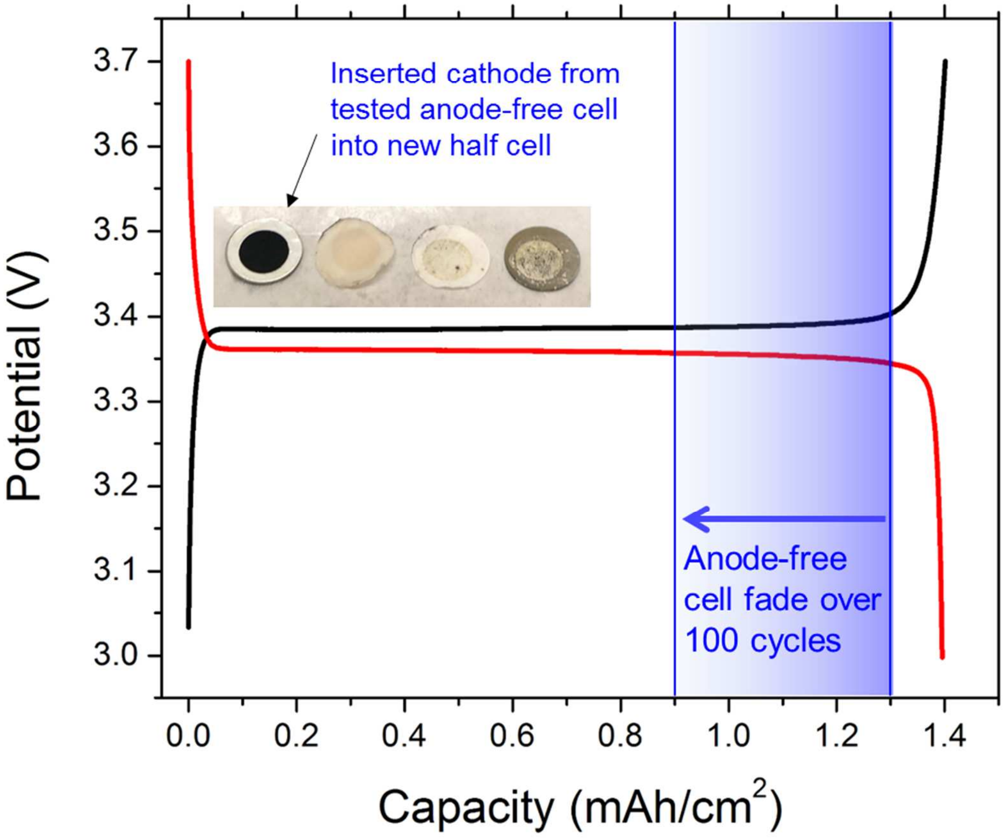

Figure S13. Potential profile of cathode from cell cycled 100+ times at 0.25 mA/cm^2 that was inserted back into a new half cell, indicating capacity fade during cycling was due to a loss of sodium.

References

1. Z. W. Seh, J. Sun, Y. Sun and Y. Cui, *ACS Cent. Sci.*, 2015, **1**, 449-455.
2. K. Yoshida, M. Nakamura, Y. Kazue, N. Tachikawa, S. Tsuzuki, S. Seki, K. Dokko and M. Watanabe, *J. Am. Chem. Soc.*, 2011, **133**, 13121-13129.